

1 Quasi-consistent efficient meshfree thin shell
2 formulation with naturally stabilized enforced essential
3 boundary conditions

4 Junchao Wu^{a,*}, Yangtao Xu^a, Bin Xu^a, Syed Humayun Basha^a

^a*Key Laboratory for Intelligent Infrastructure and Monitoring of Fujian Province, Key
Laboratory for Structural Engineering and Disaster Prevention of Fujian Province, College
of Civil Engineering, Huaqiao University, Xiamen, Fujian, 361021, China*

5 **Abstract**

This research proposed an efficient and quasi-consistent meshfree thin shell formulation with naturally stabilized enforcement of essential boundary conditions. Within the framework of the Hu-Washizu variational principle, a mixed formulation of displacements, strains and stresses is employed in this approach, where the displacements are discretized using meshfree shape functions, and the strains and stresses are expressed using smoothed gradients and covariant bases. The smoothed gradients satisfy the first second-order integration constraint and observed variational consistency for polynomial strains and stresses. Owing to Hu-Washizu variational principle, the essential boundary conditions automatically arise in its weak form. As a result, the suggested technique's enforcement of essential boundary conditions resembles that of the traditional Nitsche's method. Contrary to Nitsche's method, the costly higher order derivatives of conventional meshfree shape functions are replaced by the smoothed gradients with fast computation, which improve the efficiency. Meanwhile, the proposed formulation features a naturally stabilized term without adding any artificial stabilization factors, which eliminates the application of penalty method as a stabilization. Further, the efficacy of the proposed Hu-Washizu meshfree thin shell formulation is illustrated by a set of classical standard thin shell problems.

6 *Keywords:* Meshfree, Thin shell, Hu-Washizu variational principle,
7 Reproducing kernel gradient smoothing, Essential boundary condition

*Corresponding author
Email address: jcwu@hqu.edu.cn (Junchao Wu)

8 1. Introduction

9 Thin shell structures generally adhere to the Kirchhoff hypothesis [1], that
10 neglects the shear deformation can be described using Galerkin formulation
11 which requires to have at least C^1 continuity. The traditional finite element
12 methods usually have C^0 continuous shape functions, and it prefers Mindlin
13 thick shear theory, hybrid and mixed models in simulation of shell structure [2].
14 Meshfree methods [3, 4, 5] with high order smoothed shape functions have gar-
15 nered much research attention over the past thirty years. These techniques es-
16 tablished the shape functions based on a collection of dispersed nodes, and high
17 order continuity of shape functions can be easily achieved even with low-order
18 basis functions. For thin shell analysis, high order meshfree approximation can
19 also further alleviate the membrane locking caused by the mismatched approxi-
20 mation order of membrane strain and bending strain [6]. Moreover, nodal-based
21 meshfree approximations generally offer the flexibility of local refinement and
22 can relieve the burden of mesh distortion. Owing to these benefits, numerous
23 meshfree techniques have been developed and implemented in many scientific
24 and engineering fields [7, 8, 9, 10, 11, 12, 13]. However, the high order smoothed
25 meshfree shape functions accompany the enlarged and overlapping supports,
26 which may potentially cause many problems for shape functions. One of the
27 issues is the loss of the Kronecker delta property, which means that, unlike the
28 finite element methods, the necessary boundary conditions cannot be directly
29 enforced [14]. Another issue is that the variational consistency or said integra-
30 tion constraint, which is a condition that requires the formulation to exactly
31 reproduce the solution spanned by the basis functions, cannot be satisfied. This
32 issue is mainly caused by the misalignment between the numerical integration
33 domains and supports of shape functions. Thus, the shape functions exhibit a
34 piecewise nature in each integration domain. Besides, it has to be noted that
35 the traditional integration rules like Gauss scheme cannot ensure the integration
36 accuracy in Galerkin weak form [15, 16]. Therefore, variational consistency is
37 vital to the solution accuracy in the Galerkin meshfree formulations.

38 Various ways have been presented to enforce the necessary boundary for
39 Galerkin meshfree methods directly, including the boundary singular kernel
40 method [17], mixed transformation method [17], and interpolation element-free
41 method [18] for recovering shape functions' Kronecker property. However, these
42 methods were not based on variational setting and cannot guarantee variational
43 consistency. In the absence of a meshfree node, accuracy enforcement might
44 be poor. In contrast, enforcing the essential boundary conditions using a varia-
45 tional approach is preferred for Galerkin meshfree methods. The variational con-
46 sistent Lagrange multiplier approach was initially used to the Galerkin meshfree
47 method by Belytschko et al. [3]. In this method, the extra degrees of freedom
48 are used to determine the discretization of Lagrange multiplier. Ivannikov et al. [19]
49 extended this approach to geometrically nonlinear thin shells. Lu et al. [20] sug-
50 gested the modified variational essential boundary enforcement approach and
51 expressed the Lagrange multiplier by equivalent tractions to eliminate the ex-
52 cess degrees of freedom. However, the coercivity of this approach is not always

53 ensured and potentially reduces the accuracy. Zhu and Atluri [21] pioneered
 54 the penalty method for meshfree method, making it a straightforward approach
 55 to enforce essential boundary conditions via Galerkin weak form. However, the
 56 penalty method lacks variational consistency and requires experimental artificial
 57 parameters whose optimal value is hard to determine. Fernández-Méndez and
 58 Huerta [14] imposed necessary boundary conditions using Nitsche’s approach in
 59 the meshfree formulation. This approach can be seen as a hybrid combination
 60 of the modified variational method and the penalty method because the mod-
 61 ified variational method generates variational consistency through the use of a
 62 consistent term, and the penalty method is used as a stabilized term to recover
 63 the coercivity. Skatulla and Sansour [22] extended Nitsche’s thin shell analysis
 64 method and proposed an iteration algorithm to determine artificial parameters
 65 at each integration point.

66 In order to address the issue of numerical integration, a series of consis-
 67 tent integration schemes have been developed for Galerkin meshfree methods.
 68 Among these include stabilized conforming nodal integration [23], variational
 69 consistent integration [24], quadratic consistent integration [25], reproducing
 70 kernel gradient smoothing integration [26], and consistent projection integration
 71 [27]. The assumed strain approach establishes the most consistent integration
 72 scheme, while the smoothed gradient replaces the costly higher order derivatives
 73 of traditional meshfree shape functions and shows a high efficiency. Moreover,
 74 to achieve global variational consistency, a consistent essential boundary condi-
 75 tion enforcement must be combined with the consistent integration scheme. The
 76 combination of consistent integration scheme and Nitsche’s method for treating
 77 essential boundary conditions may demonstrate better performance since both
 78 the methods can satisfy the coercivity without requiring additional degrees of
 79 freedom. Nevertheless, Nitsche’s approach still retains the artificial parameters
 80 in the stabilized terms, and it is essential to remain cautious of the costly higher
 81 order derivatives, particularly for thin plate and thin shell problems. Recently,
 82 Wu et al. [28, 29] proposed an efficient and stabilized essential boundary con-
 83 dition enforcement method based upon the Hellinger-Reissner variational prin-
 84 ciple, where a mixed formulation in Hellinger-Reissner weak form recasts the
 85 reproducing kernel gradient smoothing integration. The terms required for en-
 86 forcing essential boundary conditions are identical to the Nitsche’s method, and
 87 both have consistent and stabilized terms. However, the stabilized term of this
 88 method naturally exists in the Hellinger-Reissner weak form and no longer needs
 89 the artificial parameters, even for essential boundary enforcement. Instead all
 90 of the higher order derivatives are represented by the smoothed gradients and
 91 their derivatives.

92 In this study, an efficient and stabilized variational consistent meshfree
 93 method that naturally enforces the essential boundary conditions is developed
 94 for thin shell structures. Following the concept of the Hellinger-Reissner prin-
 95 ciple base consistent meshfree method, the Hu-Washizu variational principle of
 96 complementary energy with variables of displacement, strains, and stresses were
 97 employed. The displacement is approximated by conventional meshfree shape
 98 functions, and the strains and stresses were expressed by smoothed gradients

99 with covariant bases. It is important to note that although the first second-order
 100 integration requirements were naturally embedded in the smoothed gradients,
 101 their fulfillment resulted in a quasi-satisfaction of variational consistency. This
 102 is mainly because of the non-polynomial nature of the stresses. Hu-Washizu's
 103 weak form was used to evaluate all the essential boundary conditions regard-
 104 ing displacements and rotations. This type of formulation is similar to the
 105 Nitsche's method but does not require any artificial parameters. Compared
 106 with Nitsche's method, conventional reproducing smoothed gradients and its
 107 direct derivatives replace the costly higher order derivatives. By utilizing the
 108 advantages of a replicating kernel gradient smoothing framework, the smoothed
 109 gradients showed better performance compared to conventional derivatives of
 110 shape functions, hence increasing the meshfree formulation's computational ef-
 111 ficiency.

112 The remainder of this research article is structured as follows: The kinemat-
 113 ics of the thin shell structure and the weak form of the associated Hu-Washizu
 114 principle are briefly described in Section 2. The mixed formulation regarding
 115 the displacements, strains and stresses in accordance with Hu-Washizu weak
 116 form are presented in Section 3. The discrete equilibrium equations are derived
 117 in Section 4 using the naturally occurring accommodation of essential. Subse-
 118 quently, they are compared to the equations obtained using Nitsche's method.
 119 The numerical results in Section 5 validate the efficacy of the proposed Hu-
 120 Washizu meshfree thin shell formulation. Lastly, the concluding remarks are
 121 presented in Section 6.

122 2. Hu-Washizu's formulation of complementary energy for thin shell

123 2.1. Kinematics for thin shell

124 Consider the configuration of a shell $\bar{\Omega}$, as shown in Fig. 1, which can be
 125 easily described by a parametric curvilinear coordinate system $\boldsymbol{\xi} = \{\xi^i\}_{i=1,2,3}$.
 126 The mid-surface of the shell denoted by Ω is specified by the in-plane coordinates
 127 $\boldsymbol{\xi} = \{\xi^\alpha\}_{\alpha=1,2}$, as the thickness direction of shell is by ξ^3 , $-\frac{h}{2} \leq \xi^3 \leq \frac{h}{2}$, h is
 128 the thickness of shell. In this work, Latin indices take the values from 1 to 3,
 129 and Greek indices are evaluated by 1 or 2. For the Kirchhoff hypothesis [6], the
 130 position $\mathbf{x} \in \bar{\Omega}$ is defined by linear functions with respect to ξ^3 :

$$\mathbf{x}(\xi^1, \xi^2, \xi^3) = \mathbf{r}(\xi^1, \xi^2) + \xi^3 \mathbf{a}_3(\xi^1, \xi^2) \quad (1)$$

in which \mathbf{r} means the position on the mid-surface of shell, and \mathbf{a}_3 is correspond-

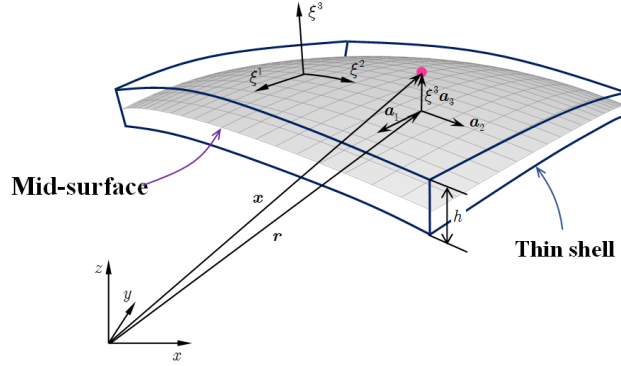


Figure 1: Kinematics for thin shell.

131 ing normal direction. For the mid-surface of shell, the in-plane covariant base
 132 vector with respect to ξ^α can be derived by a trivial partial differentiation to \mathbf{r} :
 133

$$\mathbf{a}_\alpha = \frac{\partial \mathbf{r}}{\partial \xi^\alpha} = \mathbf{r}_{,\alpha}, \alpha = 1, 2 \quad (2)$$

134 to provide for a clear expression, the subscript comma denotes the partial dif-
 135 ferentiation operation with respect to in-plane coordinates ξ^α , and the normal
 136 vector \mathbf{a}_3 can be obtained by the normalized cross product of \mathbf{a}_α 's as follows:

$$\mathbf{a}_3 = \frac{\mathbf{a}_1 \times \mathbf{a}_2}{\|\mathbf{a}_1 \times \mathbf{a}_2\|} \quad (3)$$

137 where $\|\bullet\|$ is the Euclidean norm operator.

138 With the assumption of infinitesimal deformation, the strain components
 139 with respect to the global contravariant base can be stated as:

$$\epsilon_{ij} = \frac{1}{2}(\mathbf{x}_{,i} \cdot \mathbf{u}_{,j} + \mathbf{u}_{,i} \cdot \mathbf{x}_{,j}) \quad (4)$$

where \mathbf{u} represents the displacement for the shell deformation. To satisfy the Kirchhoff hypothesis, the displacement is assumed to be of the following form:

$$\mathbf{u}(\xi^1, \xi^2, \xi^3) = \mathbf{v}(\xi^1, \xi^2) + \boldsymbol{\theta}(\xi^1, \xi^2)\xi^3 \quad (5)$$

in which the quadratic and higher order terms are neglected. \mathbf{v} , $\boldsymbol{\theta}$ represent the displacement and rotation in mid-surface, respectively.

Subsequently, plugging Eqs. (1) and (5) into Eq. (4) and neglecting the quadratic terms, the strain components can be rephrased as follows:

$$\begin{aligned} \epsilon_{\alpha\beta} &= \frac{1}{2}(\mathbf{a}_\alpha \cdot \mathbf{v}_{,\beta} + \mathbf{v}_{,\alpha} \cdot \mathbf{a}_\beta) \\ &+ \frac{1}{2}(\mathbf{a}_{3,\alpha} \cdot \mathbf{v}_{,\beta} + \mathbf{v}_{,\alpha} \cdot \mathbf{a}_{3,\beta} + \mathbf{a}_\alpha \cdot \boldsymbol{\theta}_{,\beta} + \boldsymbol{\theta}_{,\alpha} \cdot \mathbf{a}_\beta)\xi^3 \\ &= \varepsilon_{\alpha\beta} + \kappa_{\alpha\beta}\xi^3 \end{aligned} \quad (6a)$$

$$\epsilon_{\alpha 3} = \frac{1}{2}(\mathbf{a}_\alpha \cdot \boldsymbol{\theta} + \mathbf{v}_{,\alpha} \cdot \mathbf{a}_3) + \frac{1}{2}(\mathbf{a}_3 \cdot \boldsymbol{\theta})_{,\alpha}\xi^3 \quad (6b)$$

$$\epsilon_{33} = \mathbf{a}_3 \cdot \boldsymbol{\theta} \quad (6c)$$

where $\varepsilon_{\alpha\beta}$, $\kappa_{\alpha\beta}$ represent membrane and bending strains, respectively, and are given as follows:

$$\varepsilon_{\alpha\beta} = \frac{1}{2}(\mathbf{a}_\alpha \cdot \mathbf{v}_{,\beta} + \mathbf{v}_{,\alpha} \cdot \mathbf{a}_\beta) \quad (7)$$

$$\kappa_{\alpha\beta} = \frac{1}{2}(\mathbf{a}_{3,\alpha} \cdot \mathbf{v}_{,\beta} + \mathbf{v}_{,\alpha} \cdot \mathbf{a}_{3,\beta} + \mathbf{a}_\alpha \cdot \boldsymbol{\theta}_{,\beta} + \boldsymbol{\theta}_{,\alpha} \cdot \mathbf{a}_\beta) \quad (8)$$

In accordance with the Kirchhoff hypothesis, the thickness of shell will not change, and the deformation related with direction of ξ^3 will vanish, i.e. $\epsilon_{3i} = 0$. Thus, the rotation $\boldsymbol{\theta}$ can be rewritten as:

$$\epsilon_{3i} = 0 \Rightarrow \begin{cases} \boldsymbol{\theta} \cdot \mathbf{a}_\alpha = -\mathbf{v}_{,\alpha} \cdot \mathbf{a}_3 \\ \boldsymbol{\theta} \cdot \mathbf{a}_3 = 0 \end{cases} \Rightarrow \boldsymbol{\theta} = -\mathbf{v}_{,\alpha} \cdot \mathbf{a}_3 \mathbf{a}^\alpha \quad (9)$$

where \mathbf{a}^α 's is the in-plane contravariant base vector, $\mathbf{a}^\alpha \cdot \mathbf{a}_\beta = \delta^\alpha_\beta$, δ is the Kronecker delta function. The detailed derivation of Eq. 9 can be found in [30].

Furthermore, on substituting Eq. (9) into Eq. (8) leads to:

$$\kappa_{\alpha\beta} = (\Gamma_{\alpha\beta}^\gamma \mathbf{v}_{,\gamma} - \mathbf{v}_{,\alpha\beta}) \cdot \mathbf{a}_3 = -\mathbf{v}_{,\alpha}|_\beta \cdot \mathbf{a}_3 \quad (10)$$

in which $\Gamma_{\alpha\beta}^\gamma = \mathbf{a}_{\alpha,\beta} \cdot \mathbf{a}^\gamma$ is namely the Christoffel symbol of the second kind, and $\mathbf{v}_{,\alpha}|_\beta$ is the in-plane covariant derivative of $\mathbf{v}_{,\alpha}$, i.e. $\mathbf{v}_{,\alpha}|_\beta = \Gamma_{\alpha\beta}^\gamma \mathbf{v}_{,\gamma} - \mathbf{v}_{,\alpha\beta}$.

2.2. Galerkin weak form for Hu-Washizu principle of complementary energy

In this study, the Hu-Washizu variational principle of complementary energy [31] was adopted for the development of the proposed analytical approach, the

160 corresponding complementary functional, denoted by Π_C , is listed as follows:

$$\begin{aligned}
& \Pi_C(\varepsilon_{\alpha\beta}, \kappa_{\alpha\beta}, N^{\alpha\beta}, M^{\alpha\beta}) \\
&= \int_{\Omega} \frac{h}{2} \varepsilon_{\alpha\beta} C^{\alpha\beta\gamma\eta} \varepsilon_{\gamma\eta} d\Omega + \int_{\Omega} \frac{h^3}{24} \kappa_{\alpha\beta} C^{\alpha\beta\gamma\eta} \kappa_{\gamma\eta} d\Omega \\
&+ \int_{\Omega} \varepsilon_{\alpha\beta} (N^{\alpha\beta} - h C^{\alpha\beta\gamma\eta} \varepsilon_{\gamma\eta}) d\Omega + \int_{\Omega} \kappa_{\alpha\beta} (M^{\alpha\beta} - \frac{h^3}{12} C^{\alpha\beta\gamma\eta} \kappa_{\gamma\eta}) d\Omega \\
&- \int_{\Gamma_v} \mathbf{T} \cdot \bar{\mathbf{v}} d\Gamma + \int_{\Gamma_{\theta}} M_{\mathbf{n}\mathbf{n}} \bar{\theta}_{\mathbf{n}} d\Gamma - (P \mathbf{a}_3 \cdot \bar{\mathbf{v}})_{\mathbf{x} \in C_w}
\end{aligned} \tag{11}$$

161 where $C^{\alpha\beta\gamma\eta}$'s represent the components of fourth order elasticity tensor with
162 respect to the covariant base and plane stress assumption, and it can be ex-
163 pressed by Young's modulus E , Poisson's ratio ν and the in-plane contravariant
164 metric coefficients $a^{\alpha\beta}$'s, $a^{\alpha\beta} = \mathbf{a}^{\alpha} \cdot \mathbf{a}^{\beta}$, as follows:

$$C^{\alpha\beta\gamma\eta} = \frac{E}{2(1+\nu)} (a^{\alpha\gamma} a^{\beta\eta} + a^{\alpha\eta} a^{\beta\gamma} + \frac{2\nu}{1-\nu} a^{\alpha\beta} a^{\gamma\eta}) \tag{12}$$

165 and $N^{\alpha\beta}$, $M^{\alpha\beta}$ represent the components of membrane- and bending- stresses
166 which are given by:

$$N^{\alpha\beta} = h C^{\alpha\beta\gamma\eta} \varepsilon_{\gamma\eta}, \quad M^{\alpha\beta} = \frac{h^3}{12} C^{\alpha\beta\gamma\eta} \kappa_{\gamma\eta} \tag{13}$$

167 Essential boundaries on the edges and corners denoted by Γ_v , Γ_{θ} and C_v
168 are naturally existed in complementary energy functional, and $\bar{\mathbf{v}}$, $\bar{\theta}_{\mathbf{n}}$ are the
169 corresponding prescribed displacement and normal rotation, respectively. \mathbf{T} ,
170 $M_{\mathbf{n}\mathbf{n}}$ and P can be determined by Euler-Lagrange equations of shell problem
171 [30] as follows:

$$\mathbf{T} = \mathbf{T}_N + \mathbf{T}_M \rightarrow \begin{cases} \mathbf{T}_N = \mathbf{a}_{\alpha} N^{\alpha\beta} n_{\beta} \\ \mathbf{T}_M = (\mathbf{a}_3 M^{\alpha\beta} s_{\alpha} n_{\beta})_{,\gamma} s^{\gamma} + (\mathbf{a}_3 M^{\alpha\beta})|_{\beta} n_{\alpha} \end{cases} \tag{14}$$

$$M_{\mathbf{n}\mathbf{n}} = M^{\alpha\beta} n_{\alpha} n_{\beta} \tag{15}$$

$$P = -[[M^{\alpha\beta} s_{\alpha} n_{\beta}]] \tag{16}$$

174 where $\mathbf{n} = n^{\alpha} \mathbf{a}_{\alpha} = n_{\alpha} \mathbf{a}^{\alpha}$ and $\mathbf{s} = s^{\alpha} \mathbf{a}_{\alpha} = s_{\alpha} \mathbf{a}^{\alpha}$ are the outward normal and
175 tangent directions on boundaries. $[[f]]$ is the jump operator defined by:

$$[[f]]_{\mathbf{x}=\mathbf{x}_c} = \lim_{\epsilon \rightarrow \mathbf{0}^+} (f(\mathbf{x}_c + \epsilon) - f(\mathbf{x}_c - \epsilon)), \mathbf{x}_c \in \Gamma \tag{17}$$

176 where f is an arbitrary function on Γ .

177 Moreover, the natural boundary conditions should be applied by Lagrangian
178 multiplier method with displacement \mathbf{v} regarded as multiplier. Thus, then the

new complementary energy functional namely Π is given by:

$$\begin{aligned} & \Pi(\mathbf{v}, \varepsilon_{\alpha\beta}, \kappa_{\alpha\beta}, N^{\alpha\beta}, M^{\alpha\beta}) \\ &= \Pi_C(\varepsilon_{\alpha\beta}, \kappa_{\alpha\beta}, N^{\alpha\beta}, M^{\alpha\beta}) + \int_{\Gamma_M} \theta_{\mathbf{n}}(M_{\mathbf{n}\mathbf{n}} - \bar{M}_{\mathbf{n}\mathbf{n}}) d\Gamma \\ & - \int_{\Gamma_T} \mathbf{v} \cdot (\mathbf{T} - \bar{\mathbf{T}}) d\Gamma - \mathbf{v} \cdot \mathbf{a}_3(P - \bar{P})_{\mathbf{x} \in C_P} - \int_{\Omega} \mathbf{v} \cdot (\mathbf{b} - \bar{\mathbf{b}}) d\Omega \end{aligned} \quad (18)$$

where $\bar{\mathbf{T}}$, $\bar{M}_{\mathbf{n}\mathbf{n}}$ and \bar{P} are the prescribed traction, bending moment and concentrated force on edges Γ_T , Γ_M and corner C_P respectively. All the specified boundaries meet the following geometric relationships:

$$\begin{cases} \Gamma = \Gamma_v \cup \Gamma_T \cup \Gamma_\theta \cup \Gamma_M, & C = C_v \cup C_P, \\ \Gamma_v \cap \Gamma_T = \Gamma_\theta \cap \Gamma_M = C_v \cap C_P = \emptyset \end{cases} \quad (19)$$

and $\bar{\mathbf{b}}$ stands for the prescribed body force in Ω , \mathbf{b} can be written based on Euler-Lagrange equations [30] as:

$$\mathbf{b} = \mathbf{b}_N + \mathbf{b}_M \rightarrow \begin{cases} \mathbf{b}_N = (\mathbf{a}_\alpha N^{\alpha\beta})|_\beta \\ \mathbf{b}_M = (\mathbf{a}_3 M^{\alpha\beta})|_{\alpha\beta} \end{cases} \quad (20)$$

Introducing a standard variational argument to Eq. (18), $\delta\Pi = 0$, and considering the arbitrariness of virtual variables, $\delta\mathbf{v}$, $\delta\varepsilon_{\alpha\beta}$, $\delta\kappa_{\alpha\beta}$, $N^{\alpha\beta}$, $M^{\alpha\beta}$ lead to the following weak form:

$$- \int_{\Omega} h \delta\varepsilon_{\alpha\beta} C^{\alpha\beta\gamma\eta} \varepsilon_{\gamma\eta} d\Omega + \int_{\Omega} \delta\varepsilon_{\alpha\beta} N^{\alpha\beta} d\Omega = 0 \quad (21a)$$

$$- \int_{\Omega} \frac{h^3}{12} \delta\kappa_{\alpha\beta} C^{\alpha\beta\gamma\eta} \kappa_{\gamma\eta} d\Omega + \int_{\Omega} \delta\kappa_{\alpha\beta} M^{\alpha\beta} d\Omega = 0 \quad (21b)$$

$$\begin{aligned} & \int_{\Omega} \delta N^{\alpha\beta} \varepsilon_{\alpha\beta} d\Omega - \int_{\Gamma} \delta \mathbf{T}_N \cdot \mathbf{v} d\Gamma + \int_{\Omega} \delta \mathbf{b}_N \cdot \mathbf{v} d\Omega \\ & + \int_{\Gamma_v} \delta \mathbf{T}_N \cdot \mathbf{v} d\Gamma = \int_{\Gamma_v} \delta \mathbf{T}_N \cdot \bar{\mathbf{v}} d\Gamma \end{aligned} \quad (21c)$$

$$\begin{aligned} & \int_{\Omega} \delta M^{\alpha\beta} \kappa_{\alpha\beta} d\Omega - \int_{\Gamma} \delta M_{\mathbf{n}\mathbf{n}} \theta_{\mathbf{n}} d\Gamma + \int_{\Gamma} \delta \mathbf{T}_M \cdot \mathbf{v} d\Gamma + (\delta P \mathbf{a}_3 \cdot \mathbf{v})_{\mathbf{x} \in C} + \int_{\Omega} \delta \mathbf{b}_M \cdot \mathbf{v} d\Omega \\ & + \int_{\Gamma_\theta} \delta M_{\mathbf{n}\mathbf{n}} \theta_{\mathbf{n}} d\Gamma - \int_{\Gamma_v} \delta \mathbf{T}_M \cdot \mathbf{v} d\Gamma - (\delta P \mathbf{a}_3 \cdot \mathbf{v})_{\mathbf{x} \in C_v} \\ & = \int_{\Gamma_\theta} \delta M_{\mathbf{n}\mathbf{n}} \bar{\theta}_{\mathbf{n}} d\Gamma - \int_{\Gamma_v} \delta \mathbf{T}_M \cdot \bar{\mathbf{v}} d\Gamma - (\delta P \mathbf{a}_3 \cdot \bar{\mathbf{v}})_{\mathbf{x} \in C_v} \end{aligned} \quad (21d)$$

$$\begin{aligned}
& \int_{\Gamma} \delta \theta_{\mathbf{n}} M_{\mathbf{nn}} d\Gamma - \int_{\Gamma} \delta \mathbf{v} \cdot \mathbf{T} d\Gamma - (\delta \mathbf{v} \cdot \mathbf{a}_3 P)_{\mathbf{x} \in C} + \int_{\Omega} \delta \mathbf{v} \cdot \mathbf{b} d\Omega \\
& - \int_{\Gamma_{\theta}} \delta \theta_{\mathbf{n}} M_{\mathbf{nn}} d\Gamma + \int_{\Gamma_v} \delta \mathbf{v} \cdot \mathbf{T} d\Gamma + (\delta \mathbf{v} \cdot \mathbf{a}_3 P)_{\mathbf{x} \in C_v} = - \int_{\Gamma_T} \delta \mathbf{v} \cdot \bar{\mathbf{t}} d\Gamma - \int_{\Omega} \delta \mathbf{v} \cdot \bar{\mathbf{b}} d\Omega
\end{aligned} \tag{21e}$$

¹⁹² where the geometric relationships of Eq. (19) is used herein.

193 3. Mixed meshfree formulation for modified Hu-Washizu's weak form

194 3.1. Reproducing kernel approximation for displacement

195 This study approximates the displacement by adopting reproducing kernel
 196 approximation. As shown in Fig. 2, the mid-surface of the shell Ω is discretized
 197 by a set of meshfree nodes $\{\boldsymbol{\xi}_I\}_{I=1}^{n_p}$ in parametric configuration, where n_p is the
 198 total number of meshfree nodes. The approximated displacement namely \mathbf{v}^h
 199 can be expressed as:

$$\mathbf{v}(\boldsymbol{\xi}) = \sum_{I=1}^{n_p} \Psi_I(\boldsymbol{\xi}) \mathbf{d}_I \quad (22)$$

200 where Ψ_I and \mathbf{d}_I represent the shape function and nodal coefficient tensor re-
 201 lated by node $\boldsymbol{\xi}_I$. According to reproducing kernel approximation [4], the shape
 202 function takes the following form:

$$\Psi_I(\boldsymbol{\xi}) = \mathbf{p}^T(\boldsymbol{\xi}) \mathbf{c}(\boldsymbol{\xi}) \phi(\boldsymbol{\xi}_I - \boldsymbol{\xi}) \quad (23)$$

203 where \mathbf{p} is the basis function vector represented using the following quadratic
 204 function as:

$$\mathbf{p} = \{1, \xi^1, \xi^2, (\xi^1)^2, \xi^1 \xi^2, (\xi^2)^2\}^T \quad (24)$$

205 The kernel function denoted by ϕ controls the support and smoothness of
 206 meshfree shape functions. The quintic B-spline function with square support is
 207 used herein as the kernel function:

$$\phi(\boldsymbol{\xi}_I - \boldsymbol{\xi}) = \phi(\hat{s}_1) \phi(\hat{s}_2), \quad \hat{s}_\alpha = \frac{|\xi_I^\alpha - \xi^\alpha|}{s_{\alpha I}} \quad (25)$$

208 with

$$\phi(\hat{s}_\alpha) = \frac{1}{5!} \begin{cases} (3 - 3\hat{s}_\alpha)^5 - 6(2 - 3\hat{s}_\alpha)^5 + 15(1 - 3\hat{s}_\alpha)^5 & \hat{s}_\alpha \leq \frac{1}{3} \\ (3 - 3\hat{s}_\alpha)^5 - 6(2 - 3\hat{s}_\alpha)^5 & \frac{1}{3} < \hat{s}_\alpha \leq \frac{2}{3} \\ (3 - 3\hat{s}_\alpha)^5 & \frac{2}{3} < \hat{s}_\alpha \leq 1 \\ 0 & \hat{s}_\alpha > 1 \end{cases} \quad (26)$$

209 and $s_{\alpha I}$ means the support size of meshfree shape function Ψ_I .

210 The unknown vector \mathbf{c} in shape function are determined by the fulfillment
 211 of the so-called consistency condition:

$$\sum_{I=1}^{n_p} \Psi_I(\boldsymbol{\xi}) \mathbf{p}(\boldsymbol{\xi}_I) = \mathbf{p}(\boldsymbol{\xi}) \quad (27)$$

212 or equivalently

$$\sum_{I=1}^{n_p} \Psi_I(\boldsymbol{\xi}) \mathbf{p}(\boldsymbol{\xi}_I - \boldsymbol{\xi}) = \mathbf{p}(\mathbf{0}) \quad (28)$$

213 Substituting Eq. (22) into (28), yields:

$$\mathbf{A}(\boldsymbol{\xi}) \mathbf{c}(\boldsymbol{\xi}) = \mathbf{p}(\mathbf{0}) \quad \Rightarrow \quad \mathbf{c}(\boldsymbol{\xi}) = \mathbf{A}^{-1}(\boldsymbol{\xi}) \mathbf{p}(\mathbf{0}) \quad (29)$$

214 where \mathbf{A} is the moment matrix:

$$\mathbf{A}(\boldsymbol{\xi}) = \sum_{I=1}^{n_p} \phi(\boldsymbol{\xi}_I - \boldsymbol{\xi}) \mathbf{p}(\boldsymbol{\xi}_I - \boldsymbol{\xi}) \mathbf{p}^T(\boldsymbol{\xi}_I - \boldsymbol{\xi}) \quad (30)$$

215 Substituting Eq. (29) back into Eq. (22), the expression of meshfree shape
216 function can be written as:

$$\Psi_I(\boldsymbol{\xi}) = \mathbf{p}^T(\boldsymbol{\xi}_I - \boldsymbol{\xi}) \mathbf{A}^{-1}(\boldsymbol{\xi}) \mathbf{p}(\mathbf{0}) \phi(\boldsymbol{\xi}_I - \boldsymbol{\xi}) \quad (31)$$

217 3.2. Reproducing kernel gradient smoothing approximation for effective stress 218 and strain

219 In Galerkin meshfree formulation, the mid-plane of thin shell Ω is split by
220 a set of integration cells Ω_C 's, $\cup_{C=1}^{n_c} \Omega_C \approx \Omega$, as shown in Fig. 2. With the
221 inspiration of reproducing kernel smoothing framework, the Cartesian and co-
222 variant derivatives of displacement, $\mathbf{v}_{,\alpha}$ and $-\mathbf{v}_{,\alpha}|_{\beta}$, in strains $\varepsilon_{\alpha\beta}$, $\kappa_{\alpha\beta}$ are
223 approximated by $(p-1)$ -th order polynomials in each integration cells. In inte-
224 gration cell Ω_C , the approximated derivatives and strains denoted by $\mathbf{v}_{,\alpha}^h$, $\varepsilon_{\alpha\beta}^h$
225 and $-\mathbf{v}_{,\alpha}^h|_{\beta}$, $\kappa_{\alpha\beta}^h$ can be expressed by:

$$\mathbf{v}_{,\alpha}^h(\boldsymbol{\xi}) = \mathbf{q}^T(\boldsymbol{\xi}) \mathbf{d}_{\alpha}^{\varepsilon}, \quad \varepsilon_{\alpha\beta}^h(\boldsymbol{\xi}) = \mathbf{q}^T(\boldsymbol{\xi}) \frac{1}{2} (\mathbf{a}_{\alpha} \cdot \mathbf{d}_{\beta}^{\varepsilon} + \mathbf{a}_{\beta} \cdot \mathbf{d}_{\alpha}^{\varepsilon}) \quad (32)$$

$$-\mathbf{v}_{,\alpha}^h|_{\beta}(\boldsymbol{\xi}) = \mathbf{q}^T(\boldsymbol{\xi}) \mathbf{d}_{\alpha\beta}^{\kappa}, \quad \kappa_{\alpha\beta}^h(\boldsymbol{\xi}) = \mathbf{q}^T(\boldsymbol{\xi}) \mathbf{a}_3 \cdot \mathbf{d}_{\alpha\beta}^{\kappa} \quad (33)$$

227 where \mathbf{q} is the linear polynomial vector and has the following form:

$$\mathbf{q} = \{1, \xi^1, \xi^2\}^T \quad (34)$$

228 and the $\mathbf{d}_{\alpha}^{\varepsilon}$, $\mathbf{d}_{\alpha\beta}^{\kappa}$ are the corresponding coefficient vector tensors. For the con-
229 ciseness, the mixed usage of tensor and vector is introduced in this study. For
230 instance, the component of coefficient tensor vector $\mathbf{d}_{\alpha I}^{\varepsilon}$, $\mathbf{d}_{\alpha}^{\varepsilon} = \{\mathbf{d}_{\alpha I}^{\varepsilon}\}$, is a three
231 dimensional tensor, $\dim \mathbf{d}_{\alpha I}^{\varepsilon} = \dim \mathbf{v}$.

232 To satisfy the integration constraint of thin shell problem, the approximated
233 stresses $N^{\alpha\beta h}$, $M^{\alpha\beta h}$ were assumed to have a comparable form to strains, and
234 yields:

$$N^{\alpha\beta h}(\boldsymbol{\xi}) = \mathbf{q}^T(\boldsymbol{\xi}) \mathbf{a}^{\alpha} \cdot \mathbf{d}_N^{\beta}, \quad \mathbf{a}_{\alpha} N^{\alpha\beta h}(\boldsymbol{\xi}) = \mathbf{q}^T(\boldsymbol{\xi}) \mathbf{d}_N^{\beta} \quad (35)$$

$$M^{\alpha\beta h}(\boldsymbol{\xi}) = \mathbf{q}^T(\boldsymbol{\xi}) \mathbf{a}_3 \cdot \mathbf{d}_M^{\alpha\beta}, \quad \mathbf{a}_3 M^{\alpha\beta h}(\boldsymbol{\xi}) = \mathbf{q}^T(\boldsymbol{\xi}) \mathbf{d}_M^{\alpha\beta} \quad (36)$$

236 substituting the approximations of Eqs. (22), (32), (33), (35), (36) into Eqs.
237 (21c), (21d) can express $\mathbf{d}_{\beta}^{\varepsilon}$ and $\mathbf{d}_{\alpha\beta}^{\kappa}$ by \mathbf{d} as:

$$\mathbf{d}_{\beta}^{\varepsilon} = \mathbf{G}^{-1} \left(\sum_{I=1}^{n_p} (\tilde{\mathbf{g}}_{\beta I} - \bar{\mathbf{g}}_{\beta I}) \mathbf{d}_I + \hat{\mathbf{g}}_{\beta} \right) \quad (37)$$

$$\mathbf{d}_{\alpha\beta}^{\kappa} = \mathbf{G}^{-1} \left(\sum_{I=1}^{n_p} (\tilde{\mathbf{g}}_{\alpha\beta I} - \bar{\mathbf{g}}_{\alpha\beta I}) \mathbf{d}_I + \hat{\mathbf{g}}_{\alpha\beta} \right) \quad (38)$$

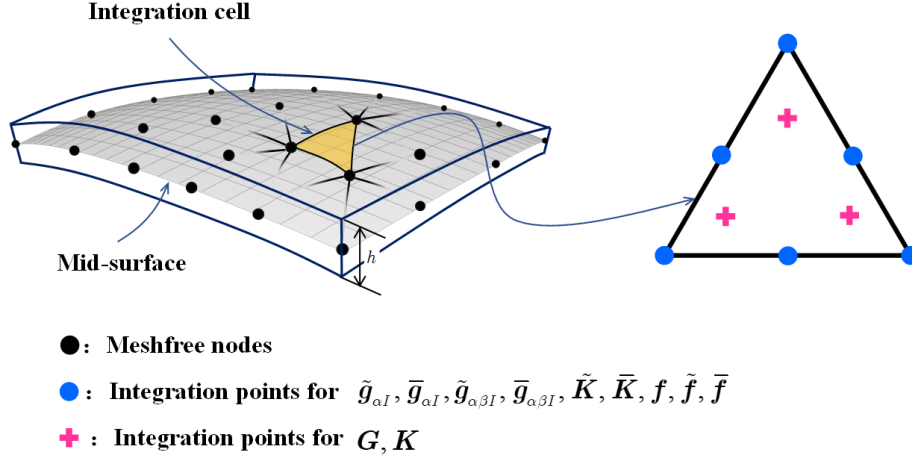


Figure 2: Integration scheme for Hu-Washizu weak form.

239 with

$$G = \int_{\Omega_C} \mathbf{q}^T \mathbf{q} d\Omega \quad (39)$$

240

$$\tilde{g}_{\beta I} = \int_{\Gamma_C} \Psi_I \mathbf{q} n_\beta d\Gamma - \int_{\Omega_C} \Psi_I \mathbf{q}_{|\beta} d\Omega \quad (40a)$$

$$\bar{g}_{\beta I} = \int_{\Gamma_C \cap \Gamma_v} \Psi_I \mathbf{q} n_\beta d\Gamma \quad (40b)$$

$$\hat{g}_\beta = \int_{\Gamma_C \cap \Gamma_v} \mathbf{q} n_\beta \bar{v} d\Gamma \quad (40c)$$

241

$$\begin{aligned} \tilde{g}_{\alpha\beta I} &= \int_{\Gamma_C} \Psi_{I,\gamma} n^\gamma \mathbf{q} n_\alpha n_\beta d\Gamma - \int_{\Gamma_C} \Psi_I (\mathbf{q}_{|\beta} n_\alpha + (\mathbf{q} s_\alpha n_\beta)_{,\gamma} s^\gamma) d\Gamma \\ &\quad + [[\Psi_I \mathbf{q} s_\alpha n_\beta]]_{\mathbf{x} \in C_C} - \int_{\Omega_C} \Psi \mathbf{q}_{,\alpha|\beta} d\Omega \end{aligned} \quad (41a)$$

$$\begin{aligned} \bar{g}_{\alpha\beta I} &= \int_{\Gamma_C \cap \Gamma_\theta} \Psi_{I,\gamma} n^\gamma \mathbf{q} n_\alpha n_\beta d\Gamma - \int_{\Gamma_C \cap \Gamma_v} \Psi_I (\mathbf{q}_{|\beta} n_\alpha + (\mathbf{q} s_\alpha n_\beta)_{,\gamma} s^\gamma) d\Gamma \\ &\quad + [[\Psi_I \mathbf{q} s_\alpha n_\beta]]_{\mathbf{x} \in C_C \cap C_v} \end{aligned} \quad (41b)$$

$$\begin{aligned} \hat{g}_{\alpha\beta} &= \int_{\Gamma_C \cap \Gamma_\theta} \mathbf{q} n_\alpha n_\beta \mathbf{a}_3 \bar{\theta} d\Gamma - \int_{\Gamma_C \cap \Gamma_v} (\mathbf{q}_{|\beta} n_\alpha + (\mathbf{q} s_\alpha n_\beta)_{,\gamma} s^\gamma) \bar{v} d\Gamma \\ &\quad + [[\mathbf{q} s_\alpha n_\beta \bar{v}]]_{\mathbf{x} \in C_C \cap C_v} \end{aligned} \quad (41c)$$

242 where evaluations of $\mathbf{q}_{|\beta}$, $\mathbf{q}_{,\alpha|\beta}$ are discussed in Appendix A. Further plugging
 243 Eqs. (37) and (38) back into Eqs. (32) and (33) respectively gives the final

244 expression of $\mathbf{v}_{,\alpha}^h$, $\varepsilon_{\alpha\beta}^h$ and $-\mathbf{v}_{,\alpha}^h|_{\beta}$, $\kappa_{\alpha\beta}^h$ as:

$$\mathbf{v}_{,\alpha}^h = \sum_{I=1}^{n_p} (\tilde{\Psi}_{I,\alpha} - \bar{\Psi}_{I,\alpha}) \mathbf{d}_I + \mathbf{q}^T \mathbf{G}^{-1} \hat{\mathbf{g}}_{\alpha} \quad (42a)$$

$$\begin{aligned} \varepsilon_{\alpha\beta}^h &= \sum_{I=1}^{n_p} \frac{1}{2} (\mathbf{a}_{\alpha} \tilde{\Psi}_{I,\beta} + \mathbf{a}_{\beta} \tilde{\Psi}_{I,\alpha}) \cdot \mathbf{d}_I - \sum_{I=1}^{n_p} \frac{1}{2} (\mathbf{a}_{\alpha} \bar{\Psi}_{I,\beta} + \mathbf{a}_{\beta} \bar{\Psi}_{I,\alpha}) \cdot \mathbf{d}_I \\ &\quad + \mathbf{q}^T \mathbf{G}^{-1} \frac{1}{2} (\mathbf{a}_{\alpha} \cdot \hat{\mathbf{g}}_{\beta} + \mathbf{a}_{\beta} \cdot \hat{\mathbf{g}}_{\alpha}) \\ &= \tilde{\varepsilon}_{\alpha\beta}^h - \bar{\varepsilon}_{\alpha\beta}^h + \hat{\varepsilon}_{\alpha\beta}^h \end{aligned} \quad (42b)$$

$$-\mathbf{v}_{,\alpha}^h|_{\beta} = \sum_{I=1}^{n_p} (\tilde{\Psi}_{I,\alpha\beta} - \bar{\Psi}_{I,\alpha\beta}) \mathbf{d}_I + \mathbf{q}^T \mathbf{G}^{-1} \hat{\mathbf{g}}_{\alpha\beta} \quad (43a)$$

$$\begin{aligned} \kappa_{\alpha\beta}^h &= \sum_{I=1}^{n_p} \tilde{\Psi}_{I,\alpha\beta} \mathbf{a}_3 \cdot \mathbf{d}_I - \sum_{I=1}^{n_p} \bar{\Psi}_{I,\alpha\beta} \mathbf{a}_3 \cdot \mathbf{d}_I + \mathbf{q}^T \mathbf{G}^{-1} \mathbf{a}_3 \cdot \hat{\mathbf{g}}_{\alpha\beta} \\ &= \tilde{\kappa}_{\alpha\beta}^h - \bar{\kappa}_{\alpha\beta}^h + \hat{\kappa}_{\alpha\beta}^h \end{aligned} \quad (43b)$$

248 with

$$\begin{cases} \tilde{\varepsilon}_{\alpha\beta}^h = \sum_{I=1}^{n_p} \frac{1}{2} (\mathbf{a}_{\alpha} \tilde{\Psi}_{I,\beta} + \mathbf{a}_{\beta} \tilde{\Psi}_{I,\alpha}) \cdot \mathbf{d}_I = \sum_{I=1}^{n_p} \tilde{\varepsilon}_{\alpha\beta I} \cdot \mathbf{d}_I \\ \bar{\varepsilon}_{\alpha\beta}^h = \sum_{I=1}^{n_p} \frac{1}{2} (\mathbf{a}_{\alpha} \bar{\Psi}_{I,\beta} + \mathbf{a}_{\beta} \bar{\Psi}_{I,\alpha}) \cdot \mathbf{d}_I = \sum_{I=1}^{n_p} \bar{\varepsilon}_{\alpha\beta I} \cdot \mathbf{d}_I \\ \hat{\varepsilon}_{\alpha\beta}^h = \mathbf{q}^T \mathbf{G}^{-1} \frac{1}{2} (\mathbf{a}_{\alpha} \cdot \hat{\mathbf{g}}_{\beta} + \mathbf{a}_{\beta} \cdot \hat{\mathbf{g}}_{\alpha}) \end{cases} \quad (44)$$

$$\begin{cases} \tilde{\Psi}_{I,\alpha}(\boldsymbol{\xi}) = \mathbf{q}^T(\boldsymbol{\xi}) \mathbf{G}^{-1} \tilde{\mathbf{g}}_{\alpha I} \\ \bar{\Psi}_{I,\alpha}(\boldsymbol{\xi}) = \mathbf{q}^T(\boldsymbol{\xi}) \mathbf{G}^{-1} \bar{\mathbf{g}}_{\alpha I} \\ \tilde{\varepsilon}_{\alpha\beta I} = \frac{1}{2} (\mathbf{a}_{\alpha} \tilde{\Psi}_{I,\beta} + \mathbf{a}_{\beta} \tilde{\Psi}_{I,\alpha}) \\ \bar{\varepsilon}_{\alpha\beta I} = \frac{1}{2} (\mathbf{a}_{\alpha} \bar{\Psi}_{I,\beta} + \mathbf{a}_{\beta} \bar{\Psi}_{I,\alpha}) \end{cases} \quad (45)$$

$$\begin{cases} \tilde{\kappa}_{\alpha\beta}^h = \sum_{I=1}^{n_p} \tilde{\Psi}_{I,\alpha\beta} \mathbf{a}_3 \cdot \mathbf{d}_I = \sum_{I=1}^{n_p} \tilde{\kappa}_{\alpha\beta I} \cdot \mathbf{d}_I \\ \bar{\kappa}_{\alpha\beta}^h = \sum_{I=1}^{n_p} \bar{\Psi}_{I,\alpha\beta} \mathbf{a}_3 \cdot \mathbf{d}_I = \sum_{I=1}^{n_p} \bar{\kappa}_{\alpha\beta I} \cdot \mathbf{d}_I \\ \hat{\kappa}_{\alpha\beta}^h = \mathbf{q}^T \mathbf{G}^{-1} \mathbf{a}_3 \cdot \hat{\mathbf{g}}_{\alpha\beta} \end{cases} \quad (46)$$

$$\begin{cases} \tilde{\Psi}_{I,\alpha\beta}(\boldsymbol{\xi}) = \mathbf{q}^T(\boldsymbol{\xi}) \mathbf{G}^{-1} \tilde{\mathbf{g}}_{\alpha\beta I} \\ \bar{\Psi}_{I,\alpha\beta}(\boldsymbol{\xi}) = \mathbf{q}^T(\boldsymbol{\xi}) \mathbf{G}^{-1} \bar{\mathbf{g}}_{\alpha\beta I} \\ \tilde{\kappa}_{\alpha\beta I} = \tilde{\Psi}_{I,\alpha\beta} \mathbf{a}_3 \\ \bar{\kappa}_{\alpha\beta I} = \bar{\Psi}_{I,\alpha\beta} \mathbf{a}_3 \end{cases} \quad (47)$$

252 It has to be noted that, referring to reproducing kernel gradient smoothing
 253 framework [26], $\tilde{\Psi}_{I,\alpha}$, $\tilde{\Psi}_{I,\alpha\beta}$ are actually the first and second order smoothed
 254 gradients in curvilinear coordinates. If the right hand side integration constraints
 255 for first and second order gradients are $\tilde{\mathbf{g}}_{\alpha I}$ and $\tilde{\mathbf{g}}_{\alpha\beta I}$, respectively, then this for-
 256 mulation can satisfy the variational consistency for the second order polynomi-
 257 als. It should be mentioned that in curved model, the variational consistency for
 258 non-polynomial functions, such as trigonometric functions, should be required
 259 for the polynomial solution. Even with high order polynomial variational consis-
 260 tency, the proposed formulation cannot exactly reproduce the solution spanned
 261 by the basis functions. However, the accuracy of reproducing kernel smoothed
 262 gradients is still superior than the traditional meshfree formulation. The nu-
 263 merical examples in the following section will better demonstrate the precision
 264 of the reproducing kernel smoothed gradients.

265 **4. Naturally variational enforcement for essential boundary condi-**
 266 **tions**

267 *4.1. Discrete equilibrium equations*

268 With the approximated effective stresses and strains, the last equation of
 269 weak form Eq. (21e) becomes:

$$-\sum_{C=1}^{n_e} \sum_{I=1}^{n_p} \delta \mathbf{d}_I \cdot \left((\tilde{\mathbf{g}}_{\alpha I}^T - \bar{\mathbf{g}}_{\alpha I}^T) \mathbf{d}_N^\alpha + (\tilde{\mathbf{g}}_{\alpha \beta I}^T - \bar{\mathbf{g}}_{\alpha \beta I}^T) \mathbf{d}_M^{\alpha \beta} \right) = -\sum_{I=1}^{n_p} \delta \mathbf{d}_I \cdot \mathbf{f}_I \quad (48)$$

270 where \mathbf{f}_I 's denote the components of the traditional force vector:

$$\mathbf{f}_I = \int_{\Gamma_t} \Psi_I \bar{\mathbf{t}} d\Gamma - \int_{\Gamma_M} \Psi_{I,\gamma} n^\gamma \bar{M}_{nn} d\Gamma + [[\Psi_I \mathbf{a}_3 \bar{P}]]_{\mathbf{x} \in C_P} + \int_{\Omega} \Psi_I \bar{\mathbf{b}} d\Omega \quad (49)$$

271 The left side of Eq. (48) can be simplified using the following steps. For clarity,
 272 the derivation of first term in Eq. (48) taken as an example is given by:

$$\begin{aligned} \sum_{I=1}^{n_p} \delta \mathbf{d}_I \cdot \tilde{\mathbf{g}}_{\alpha I}^T \mathbf{d}_N^\alpha &= \sum_{I=1}^{n_p} \delta \mathbf{d}_I \cdot (\mathbf{G}^{-1} \tilde{\mathbf{g}}_{\alpha I})^T \mathbf{G} \mathbf{d}_N^\alpha \\ &= \int_{\Omega_C} \sum_{I=1}^{n_p} \delta \mathbf{d}_I \cdot (\mathbf{q}^T \mathbf{G}^{-1} \tilde{\mathbf{g}}_{\alpha I}) \mathbf{q}^T \mathbf{d}_N^\alpha d\Omega \\ &= \int_{\Omega_C} \sum_{I=1}^{n_p} \delta \mathbf{d}_I \cdot \mathbf{a}_\beta (\mathbf{q}^T \mathbf{G}^{-1} \tilde{\mathbf{g}}_{\alpha I}) N^{\alpha \beta h} d\Omega \\ &= \int_{\Omega_C} \delta \tilde{\varepsilon}_{\alpha \beta}^h N^{\alpha \beta h} d\Omega \end{aligned} \quad (50)$$

273 following the above procedure and including the weak form of Eqs. (21a), (21b),
 274 the left side of Eq. (48) in Ω_C becomes:

$$\begin{aligned}
 & \sum_{I=1}^{n_p} \delta \mathbf{d}_I \cdot \left((\tilde{\mathbf{g}}_{\alpha I}^T - \bar{\mathbf{g}}_{\alpha I}^T) \mathbf{d}_N^\alpha + (\tilde{\mathbf{g}}_{\alpha \beta I}^T - \bar{\mathbf{g}}_{\alpha \beta I}^T) \mathbf{d}_M^{\alpha \beta} \right) \\
 &= \int_{\Omega_C} ((\delta \tilde{\varepsilon}_{\alpha \beta}^h - \delta \bar{\varepsilon}_{\alpha \beta}^h) N^{\alpha \beta h} + (\delta \tilde{\kappa}_{\alpha \beta}^h - \delta \bar{\kappa}_{\alpha \beta}^h) M^{\alpha \beta h}) d\Omega \\
 &= \int_{\Omega_C} (\delta \tilde{\varepsilon}_{\alpha \beta}^h - \delta \bar{\varepsilon}_{\alpha \beta}^h) h C^{\alpha \beta \gamma \eta} \varepsilon_{\gamma \eta}^h + (\delta \tilde{\kappa}_{\alpha \beta}^h - \delta \bar{\kappa}_{\alpha \beta}^h) \frac{h^3}{12} C^{\alpha \beta \gamma \eta} \kappa_{\gamma \eta}^h \\
 &= \int_{\Omega_C} \delta \tilde{\varepsilon}_{\alpha \beta}^h h C^{\alpha \beta \gamma \eta} \varepsilon_{\gamma \eta}^h d\Omega + \int_{\Omega_C} \delta \tilde{\kappa}_{\alpha \beta}^h \frac{h^3}{12} C^{\alpha \beta \gamma \eta} \kappa_{\gamma \eta}^h d\Omega \\
 &\quad - \int_{\Omega_C} \delta \bar{\varepsilon}_{\alpha \beta}^h h C^{\alpha \beta \gamma \eta} \varepsilon_{\gamma \eta}^h d\Omega - \int_{\Omega_C} \delta \bar{\kappa}_{\alpha \beta}^h h C^{\alpha \beta \gamma \eta} \varepsilon_{\gamma \eta}^h d\Omega \\
 &\quad - \int_{\Omega_C} \delta \tilde{\kappa}_{\alpha \beta}^h \frac{h^3}{12} C^{\alpha \beta \gamma \eta} \kappa_{\gamma \eta}^h d\Omega - \int_{\Omega_C} \delta \bar{\kappa}_{\alpha \beta}^h \frac{h^3}{12} C^{\alpha \beta \gamma \eta} \kappa_{\gamma \eta}^h d\Omega \\
 &\quad + \int_{\Omega_C} \delta \bar{\varepsilon}_{\alpha \beta}^h h C^{\alpha \beta \gamma \eta} \varepsilon_{\gamma \eta}^h d\Omega + \int_{\Omega_C} \delta \bar{\kappa}_{\alpha \beta}^h \frac{h^3}{12} C^{\alpha \beta \gamma \eta} \kappa_{\gamma \eta}^h d\Omega \\
 &\quad + \int_{\Omega_C} (\delta \tilde{\varepsilon}_{\alpha \beta}^h - \delta \bar{\varepsilon}_{\alpha \beta}^h) h C^{\alpha \beta \gamma \eta} \varepsilon_{\gamma \eta}^h d\Omega + \int_{\Omega_C} (\delta \tilde{\kappa}_{\alpha \beta}^h - \delta \bar{\kappa}_{\alpha \beta}^h) \frac{h^3}{12} C^{\alpha \beta \gamma \eta} \kappa_{\gamma \eta}^h d\Omega
 \end{aligned} \tag{51}$$

275 The complete discrete equilibrium equations can be obtained by further substituting
 276 Eqs. (44) and (46) into above equation, respectively:

$$(\mathbf{K} + \tilde{\mathbf{K}} + \bar{\mathbf{K}}) \mathbf{d} = \mathbf{f} + \tilde{\mathbf{f}} + \bar{\mathbf{f}} \tag{52}$$

277 where the components of stiffness matrices and force vectors in discrete equilibrium
 278 equations can be evaluated as follows:

$$\mathbf{K}_{IJ} = \int_{\Omega} \tilde{\varepsilon}_{\alpha \beta I} h C^{\alpha \beta \gamma \eta} \tilde{\varepsilon}_{\gamma \eta J} d\Omega + \int_{\Omega} \tilde{\kappa}_{\alpha \beta I} \frac{h^3}{12} C^{\alpha \beta \gamma \eta} \tilde{\kappa}_{\gamma \eta J} d\Omega \tag{53}$$

279

$$\begin{aligned}
 \tilde{\mathbf{K}}_{IJ} &= - \int_{\Gamma_v} (\Psi_I \tilde{\mathbf{T}}_{NJ} + \tilde{\mathbf{T}}_{NI} \Psi_J) d\Gamma \\
 &\quad + \int_{\Gamma_\theta} (\Psi_{I,\gamma} n^\gamma \mathbf{a}_3 \tilde{\mathbf{M}}_{nnJ} + \mathbf{a}_3 \tilde{\mathbf{M}}_{nnI} \Psi_{J,\gamma} n^\gamma) d\Gamma \\
 &\quad + ([[\Psi_I \mathbf{a}_3 \tilde{\mathbf{P}}_J]] + [[\tilde{\mathbf{P}}_I \mathbf{a}_3 \Psi_J]])_{\mathbf{x} \in C_v}
 \end{aligned} \tag{54a}$$

$$\tilde{\mathbf{f}}_I = - \int_{\Gamma_v} \tilde{\mathbf{T}}_{NI} \cdot \bar{\mathbf{v}} d\Gamma + \int_{\Gamma_\theta} \tilde{\mathbf{M}}_{nnI} \bar{\theta}_n d\Gamma + [[\tilde{\mathbf{P}}_I \mathbf{a}_3 \cdot \bar{\mathbf{v}}]]_{\mathbf{x} \in C_v} \tag{54b}$$

280

$$\bar{\mathbf{K}}_{IJ} = - \int_{\Gamma_v} \bar{\mathbf{T}}_{MI} \Psi_J d\Gamma + \int_{\Gamma_\theta} \mathbf{a}_3 \bar{\mathbf{M}}_{nnI} \Psi_{J,\gamma} n^\gamma d\Gamma + [[\bar{\mathbf{P}}_I \mathbf{a}_3 \Psi_J]]_{\mathbf{x} \in C_v} \tag{55a}$$

$$\bar{\mathbf{f}}_I = - \int_{\Gamma_v} \bar{\mathbf{T}}_{MI} \cdot \bar{\mathbf{v}} d\Gamma + \int_{\Gamma_\theta} \bar{\mathbf{M}}_{nnI} \bar{\theta}_n d\Gamma + [[\bar{\mathbf{P}}_I \mathbf{a}_3 \cdot \bar{\mathbf{v}}]]_{\mathbf{x} \in C_v} \tag{55b}$$

281 The detailed derivations of Eqs (53)-(55) are listed in the Appendix B. As
 282 shown in these equations, Eq. (53) is the conventional stiffness matrix evalu-
 283 ated by smoothed gradients $\tilde{\Psi}_{I,\alpha}$, $\tilde{\Psi}_{I,\alpha|\beta}$, and the Eqs. (54) and (55) contribute
 284 for the enforcement of essential boundary. It should be noticed that, in accor-
 285 dance with reproducing kernel smoothed gradient framework, the integration
 286 scheme of Eqs. (53-55) should be aligned with those used in the construction of
 287 smoothed gradients. The integration scheme used for the proposed method is
 288 shown in Fig. 2, in which the total number of the blue circular integration points
 289 has been optimized from a global point of view, aiming to reduce the compu-
 290 tation of traditional meshfree shape functions and its first order derivatives. In
 291 contrast, for assembly stiffness matrix \mathbf{K} , the low order Gauss integration rule
 292 is suitable to ensure the accuracy due to the inherently variational consistency
 293 in the smoothed gradients. The detailed positions and weight of the integration
 294 points and the efficiency demonstration of this optimized integration scheme
 295 can be found in [26, 32]. Examining Eqs. (54) and (55), closely reveal that the
 296 structure of the suggested approach to enforce essential boundary conditions is
 297 identical to that of the conventional Nitsche's method, with both having the
 298 consistent and stabilized terms. Thus, a review of Nitsche's method and a com-
 299 parison with the proposed approach will be provided in the next subsection.

300 4.2. Comparison with Nitsche's method

301 The Nitsche's method for enforcing essential boundaries can be regarded as a
 302 combination of Lagrangian multiplier method and penalty method, in which the
 303 Lagrangian multiplier is represented by the approximated displacement. The
 304 corresponding total potential energy functional Π_P is given by:

$$\begin{aligned}
 \Pi_P(\mathbf{v}) = & \int_{\Omega} \frac{1}{2} \varepsilon_{\alpha\beta} N^{\alpha\beta} d\Omega + \int_{\Omega} \frac{1}{2} \kappa_{\alpha\beta} M^{\alpha\beta} d\Omega \\
 & - \int_{\Gamma_t} \mathbf{v} \cdot \bar{\mathbf{t}} d\Gamma + \int_{\Gamma_M} \mathbf{v}_{,\gamma} n^{\gamma} \mathbf{a}_3 M_{nn} d\Gamma + (\mathbf{v} \cdot \mathbf{a}_3 P)_{\mathbf{x} \in C_P} - \int_{\Omega} \mathbf{v} \cdot \bar{\mathbf{b}} d\Omega \\
 & - \underbrace{\int_{\Gamma_v} \mathbf{t} \cdot (\mathbf{v} - \bar{\mathbf{v}}) d\Gamma + \int_{\Gamma_{\theta}} M_{nn} (\theta_n - \bar{\theta}_n) d\Gamma + (P \mathbf{a}_3 \cdot (\mathbf{v} - \bar{\mathbf{v}}))_{\mathbf{x} \in C_v}}_{\text{consistent term}} \quad (56) \\
 & + \underbrace{\sum_{i=1}^3 \frac{\alpha_{vi}}{2} \int_{\Gamma_v} (\mathbf{v} \cdot \mathbf{a}_i)^2 d\Gamma + \frac{\alpha_{\theta}}{2} \int_{\Gamma_{\theta}} \theta_n^2 d\Gamma + \frac{\alpha_C}{2} (\mathbf{v} \cdot \mathbf{a}_3)_{\mathbf{x} \in C_v}^2}_{\text{stabilized term}}
 \end{aligned}$$

305 where the consistent term generated from the Lagrangian multiplier method
 306 contributes to enforce the essential boundary, and meet the variational con-
 307 sistency condition. However, the consistent term can not always ensure the
 308 coercivity of stiffness, so the penalty method is introduced to serve as a sta-
 309 bilized term, in which α_{vi} is the experimental artificial parameter to enforce
 310 the displacement towards the \mathbf{a}_i direction, α_{θ} and α_C are parameters to en-
 311 force rotation and corner deflection, respectively. With a standard variational

argument, the corresponding weak form can be stated as:

$$\begin{aligned}
\delta \Pi_P(\mathbf{v}) = & \int_{\Omega} \delta \varepsilon_{\alpha\beta} N^{\alpha\beta} d\Omega + \int_{\Omega} \delta \kappa_{\alpha\beta} M^{\alpha\beta} d\Omega \\
& - \int_{\Gamma_t} \delta \mathbf{v} \cdot \bar{\mathbf{t}} d\Gamma + \int_{\Gamma_M} \delta \mathbf{v}_{,\gamma} n^{\gamma} \mathbf{a}_3 M_{nn} d\Gamma + (\delta \mathbf{v} \cdot \mathbf{a}_3 P)_{\mathbf{x} \in C_P} - \int_{\Omega} \delta \mathbf{v} \cdot \bar{\mathbf{b}} d\Omega \\
& - \int_{\Gamma_v} \delta \mathbf{v} \cdot \mathbf{t} d\Gamma + \int_{\Gamma_{\theta}} \delta \theta_{\mathbf{n}} M_{nn} d\Gamma + (\mathbf{v} \cdot \mathbf{a}_3 P)_{\mathbf{x} \in C_v} \\
& - \int_{\Gamma_v} \delta \mathbf{t} \cdot (\mathbf{v} - \bar{\mathbf{v}}) d\Gamma + \int_{\Gamma_{\theta}} \delta M_{nn} (\theta_{\mathbf{n}} - \bar{\theta}_{\mathbf{n}}) d\Gamma + (\delta P \mathbf{a}_3 \cdot (\mathbf{v} - \bar{\mathbf{v}}))_{\mathbf{x} \in C_v} \\
& + \sum_{i=1}^3 \alpha_{vi} \int_{\Gamma_v} (\delta \mathbf{v} \cdot \mathbf{a}_i) (\mathbf{a}_i \cdot \mathbf{v}) d\Gamma + \alpha_{\theta} \int_{\Gamma_{\theta}} \delta \theta_{\mathbf{n}} \theta_{\mathbf{n}} d\Gamma + \alpha_C (\delta \mathbf{v} \cdot \mathbf{a}_3 \mathbf{a}_3 \cdot \mathbf{v})_{\mathbf{x} \in C_v} \\
& = 0
\end{aligned} \tag{57}$$

Upon further invoking the conventional reproducing kernel approximation of Eq. (22), the subsequent discrete equilibrium equations can be obtained:

$$(\mathbf{K} + \mathbf{K}^c + \mathbf{K}^s) \mathbf{d} = \mathbf{f} + \mathbf{f}^c + \mathbf{f}^s \tag{58}$$

where the stiffness \mathbf{K} is identical with Eq. (53). \mathbf{K}^c and \mathbf{K}^s are the stiffness matrices for consistent and stabilized terms, respectively, and their components have the following form:

$$\begin{aligned}
\mathbf{K}_{IJ}^c = & - \int_{\Gamma_v} (\Psi_I \mathbf{T}_{NJ} + \mathbf{T}_{NI} \Psi_J) d\Gamma \\
& + \int_{\Gamma_{\theta}} (\Psi_{I,\gamma} n^{\gamma} \mathbf{a}_3 M_{nnJ} + \mathbf{a}_3 M_{nnI} \Psi_{J,\gamma} n^{\gamma}) d\Gamma \\
& + ([\Psi_I \mathbf{a}_3 P_J] + [P_I \mathbf{a}_3 \Psi_J])_{\mathbf{x} \in C_v}
\end{aligned} \tag{59a}$$

$$\mathbf{f}_I^c = - \int_{\Gamma_v} \mathbf{T}_I \cdot \bar{\mathbf{v}} d\Gamma + \int_{\Gamma_{\theta}} M_{nnI} \bar{\theta}_{\mathbf{n}} d\Gamma + [P_I \mathbf{a}_3 \cdot \bar{\mathbf{v}}]_{\mathbf{x} \in C_v} \tag{59b}$$

318

$$\mathbf{K}_{IJ}^s = \alpha_v \int_{\Gamma_v} \Psi_I \Psi_J d\Gamma + \alpha_{\theta} \int_{\Gamma_{\theta}} \Psi_{I,\eta} n^{\eta} \mathbf{a}_3 \mathbf{a}_3 n^{\gamma} \Psi_{J,\gamma} d\Gamma + \alpha_C [\Psi_I \mathbf{a}_3 \mathbf{a}_3 \Psi_J]_{\mathbf{x} \in C_v} \tag{60a}$$

$$\mathbf{f}_I^s = \alpha_v \int_{\Gamma_v} \Psi_I \bar{\mathbf{v}} d\Gamma + \alpha_{\theta} \int_{\Gamma_{\theta}} \Psi_{I,\eta} n^{\eta} \mathbf{a}_3 \bar{\theta}_{\mathbf{n}} d\Gamma + \alpha_C [\Psi_I \mathbf{a}_3 \mathbf{a}_3 \cdot \bar{\mathbf{v}}]_{\mathbf{x} \in C_v} \tag{60b}$$

319 with

$$\boldsymbol{\alpha}_v = \begin{bmatrix} \alpha_{v1} & 0 & 0 \\ 0 & \alpha_{v2} & 0 \\ 0 & 0 & \alpha_{v3} \end{bmatrix} \tag{61}$$

On comparing with the consistent terms of Eqs. (54) and (59), the expressions were almost identical, the major difference is that the higher order

322 derivatives of shape functions have been replaced by the smoothed gradients.
 323 Owing to the reproducing kernel framework, the construction of the smoothed
 324 gradients only concerned about the computation of traditional meshfree shape
 325 functions and their first order derivatives, which avoid the costly computation
 326 of higher order derivatives. Moreover, the stabilized terms in Eq. (60) em-
 327 ploys the penalty method with big enough artificial parameters to ensure the
 328 coercivity of stiffness. Besides, the optimal values of these artificial parame-
 329 ters are proportional to the grid size of discrete model that can be represented
 330 by the support size in meshfree approximation, where $\alpha_{v\alpha} \propto s^{-1}$, $\alpha_{v3} \propto s^{-3}$,
 331 $\alpha_\theta \propto s^{-1}$, $\alpha_C \propto s^{-2}$ [30], and $s = \min\{s_{\alpha I}\}$. In contrast, the stabilized term of
 332 Eq. (55) naturally exists in its weak form, and can stabilize the result without
 333 considering any artificial parameters.

334 5. Numerical examples

335 In this section, the suggested method is validated through several exam-
 336 ples using the Nitsche's method, the consistent reproducing kernel gradient
 337 smoothing integration scheme (RKGSI), and the non-consistent Gauss inte-
 338 gration scheme (GI) with penalty method, as well as the proposed Hu-Washizu
 339 formulation (HW) to enforce the necessary boundary conditions. A normalized
 340 support size of 2.5 is used for all the considered methods to ensure the require-
 341 ment of quadratic base meshfree approximation. To eliminate the influence of
 342 integration error, the Gauss integration scheme uses 6 Gauss points for domain
 343 integration and 3 points for boundary integration, so as to maintain the same
 344 integration accuracy between domain and boundaries. Moreover, the number
 345 of integration points are identical between the Gauss and RKGSI schemes. The
 346 error estimates of displacement (L_2 -Error) and energy (H_e -Error) is used here:

$$\begin{aligned}
 L_2\text{-Error} &= \frac{\sqrt{\int_{\Omega} (\mathbf{v} - \mathbf{v}^h) \cdot (\mathbf{v} - \mathbf{v}^h) d\Omega}}{\sqrt{\mathbf{v} \cdot \mathbf{v}}} \\
 H_e\text{-Error} &= \frac{\sqrt{\int_{\Omega} \left((\varepsilon_{\alpha\beta} - \varepsilon_{\alpha\beta}^h)(N^{\alpha\beta} - N^{\alpha\beta h}) + \int_{\Omega} (\kappa_{\alpha\beta} - \kappa_{\alpha\beta}^h)(M^{\alpha\beta} - M^{\alpha\beta h}) \right) d\Omega}}{\sqrt{\int_{\Omega} (\varepsilon_{\alpha\beta} N^{\alpha\beta} + \kappa_{\alpha\beta} M^{\alpha\beta}) d\Omega}}
 \end{aligned} \tag{62}$$

347 5.1. Patch tests

348 The linear and quadratic patch tests for flat and curved thin shells are
 349 firstly studied to verify the variational consistency of the proposed method.
 350 As shown in Fig. 3, the flat and curved models are depicted by an identical
 351 parametric domain $\Omega = (0, 1) \otimes (0, 1)$, where the cylindrical coordinate sys-
 352 tem with radius $R = 1$, thickness $h = 0.1$ is employed to describe the curved
 353 model, and the whole domain Ω is discretized by the 165 meshfree nodes. The
 354 Young's modulus and Poisson's ratio of thin shell are set to $E = 1$, $\nu = 0$.
 355 The artificial parameters of $\alpha_v = 10^5 \times E$, $\alpha_\theta = 10^3 \times E$, $\alpha_C = 10^5 \times E$
 356 and $\alpha_v = 10^9 \times E$, $\alpha_\theta = 10^9 \times E$, $\alpha_C = 10^9 \times E$ were adopted in Nitsche's-
 357 and penalty- method, respectively. All the boundaries are enforced as essential
 358 boundary conditions with the following manufactured exact solution:

$$\mathbf{v} = \begin{Bmatrix} (\xi^1 + 2\xi^2)^n \\ (3\xi^1 + 4\xi^2)^n \\ (5\xi^1 + 6\xi^2)^n \end{Bmatrix}, \quad n = \begin{cases} 1 & \text{Linear patch test} \\ 2 & \text{Quadratic patch test} \end{cases} \tag{63}$$

359 Table 1 lists the L_2 - and H_e -Error results of patch test with flat model, where
 360 the RKGSI scheme with variational consistent essential boundary enforcement,
 361 i.e. RKGSI-Nitsche and RKGSI-HW, can pass the linear and quadratic patch
 362 test. In contrast, the RKGSI-Penalty cannot pass the patch test since the
 363 Penalty method is unable to ensure the variational consistency. Due to the
 364 loss of variational consistency condition, even with the Nitsche's method, Gauss

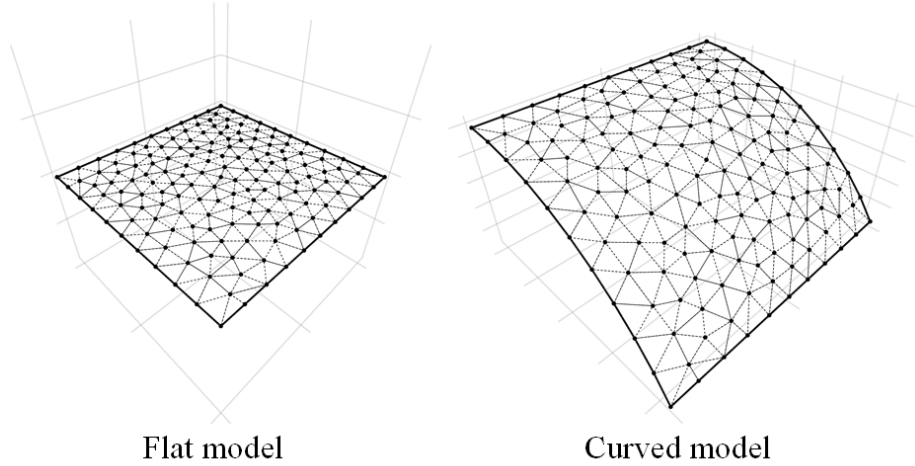


Figure 3: Meshfree discretization for patch test

365 meshfree formulations show noticeable errors. Table 2 shows the results for
 366 curved model, which indicated that all the considered methods cannot pass
 367 the patch test. This is mainly because the proposed smoothed gradient of
 368 Eqs. (35) and (36) could not exactly reproduce the non-polynomial membrane
 369 and bending stresses. On the other hand, the RKGSI-HW and RKGSI-Nitsche
 370 methods provide better accuracy compared to the other approaches due to the
 371 fulfillment of first second-order variational consistency. Even only with local
 372 variational consistency, the RKGSI-Penalty obtained a better result than the
 373 traditional Gauss scheme. Meanwhile, the bending moment contours of M^{12}
 374 are listed in Fig. 4, which further verify that the proposed method provided a
 375 satisfactory result compared to the exact solution. Contrarily, both the RKGSI-
 376 Penalty and the conventional Gauss meshree formulations observed errors.

Table 1: Results of patch test for flat model.

	Linear patch test		Quadratic patch test	
	L_2 -Error	H_e -Error	L_2 -Error	H_e -Error
GI-Penalty	4.45E-04	1.35E-02	2.01E-03	1.63E-02
GI-Nitsche	4.51E-04	1.42E-02	1.22E-03	1.68E-02
RKGSI-Penalty	3.64E-09	6.77E-08	4.54E-09	6.57E-08
RKGSI-Nitsche	3.31E-12	1.34E-11	5.98E-12	1.21E-11
RKGSI-HR	6.67E-13	1.50E-11	1.07E-12	1.26E-11

377 5.2. Scordelis-Lo roof

378 This example considers the classical Scordelis-Lo roof problem, as depicted
 379 in Fig. 5. The cylindrical roof has dimensions $R = 25$, $L = 50$, $h = 0.25$,

Table 2: Results of patch test for cylindrical model.

	Linear patch test		Quadratic patch test	
	L_2 -Error	H_e -Error	L_2 -Error	H_e -Error
GI-Penalty	3.79E-04	1.30E-02	1.74E-03	1.37E-02
GI-Nitsche	4.04E-04	1.42E-02	1.15E-03	1.49E-02
RKGSi-Penalty	1.47E-04	5.39E-03	2.26E-04	2.09E-03
RKGSi-Nitsche	2.41E-06	7.37E-05	2.47E-06	2.89E-05
RKGSi-HR	4.28E-06	1.30E-04	9.69E-06	2.41E-04

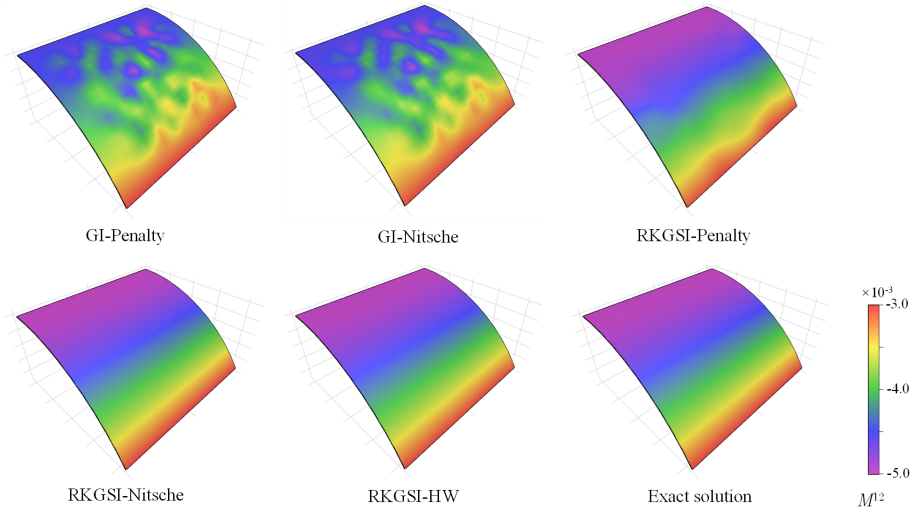


Figure 4: Contour plots of M^{12} for curved shell patch test.

380 Young's modulus $E = 4.32 \times 10^8$ and Poisson's ratio $\nu = 0.0$. The entire roof
381 is subjected to an uniform body force of $b_z = -90$, with the straight edges
382 remaining free and the the curved edges are enforced by $v_x = v_z = 0$.

383 Due to the symmetry, only a quadrant of the model is considered for meshfree
384 analysis, which is discretized by the 11×16 , 13×20 , 17×24 and 19×28 meshfree
385 nodes, as listed in Fig. 6. The comparison of the displacement in z -direction
386 at node A , v_{A3} , is used as the investigated quantity, with the reference value
387 0.3006 given by [33]. Firstly, Fig. 7 presents a sensitivity study for the artificial
388 parameters of α_{vi} 's and α_θ 's in the RKGSi meshfree formulations with the
389 Nitsche's- and penalty- method, where all of the parameters are scaled by the
390 support size as, $\alpha_{v\alpha} = s^{-1}\bar{\alpha}_v$, $\alpha_{v3} = s^{-3}\bar{\alpha}_v$ and $\alpha_\theta = s^{-1}\bar{\alpha}_\theta$. For a better
391 comparison, the result of the proposed RKGSi-HW is also listed in this figure.
392 The results of Fig. 7 revealed, that Nitsche's method observed less artificial
393 sensitivity. However, both the methods cannot trivially determine the optimal
394 values of the artificial parameters. The optimal artificial parameters from Fig.

7 are adopted for the convergence study in Fig. 8. The convergence result showed that the RKGSi method get satisfactory results while the traditional Gauss methods demonstrated noticeable errors.

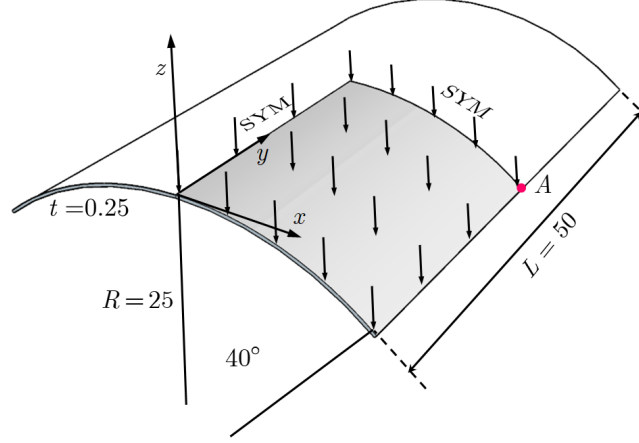


Figure 5: Description of Scordelis-Lo roof problem.

5.3. Pinched Hemispherical shell

Consider the hemispherical shell shown in Fig. 9, which is loaded at four points $P = \pm 2$ at 90° interval at its bottom. The hemispherical shell has an radius $R = 10$, thickness $h = 0.04$, Young's modulus $E = 6.825 \times 10^7$ and Poisson's ratio $\nu = 0.3$.

Due to symmetry, only quadrant model, where the 16×16 , 24×24 , 32×32 and 40×40 meshfree nodes have been discretized as shown in Fig. (10), were considered. The quantity under investigation for convergence is the displacement at x -direction on point A , $v_{A1} = 0.094$ [34]. Fig. 11 displays the corresponding convergence results, indicating the RKGSi scheme performed significantly better compared to the GI meshfree formulation. Meanwhile, the efficiency comparison for this problem is also shown in Fig. 12, in which the CPU time for assembly and calculation of shape functions are considered. Fig. 12(a) indicates that the RKGSi scheme observed high efficiency in assembly. This is due to the variational inconsistent Gauss meshfree formulation which require more Gaussian points to get satisfactory results. Fig. 12(b) lists the CPU time spent on enforcing essential boundary conditions for the penalty method, Nitsche's method and proposed HW method. The results highlighted that the proposed HW method consumed comparable CPU time in assembly compared to Nitsche's method. However, less time was spent to calculate the shape functions. Since both the HW method and penalty method were developed considering the shape functions first order derivatives. For this reason, both the methods shared an almost identical time in computing the shape functions.

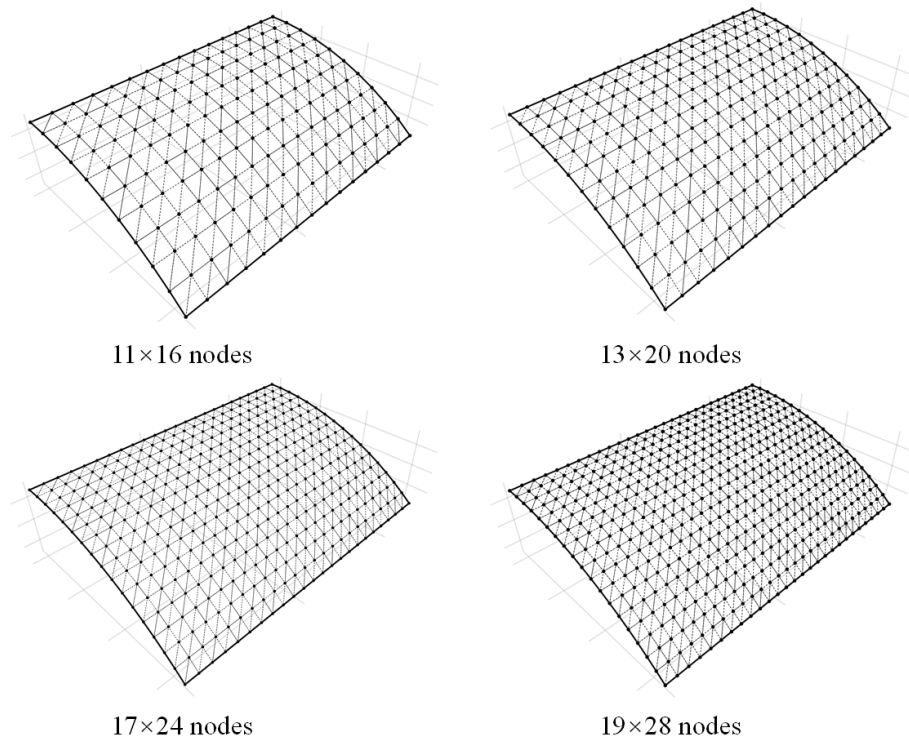


Figure 6: Meshfree discretizations for Scordelis-Lo roof problem.

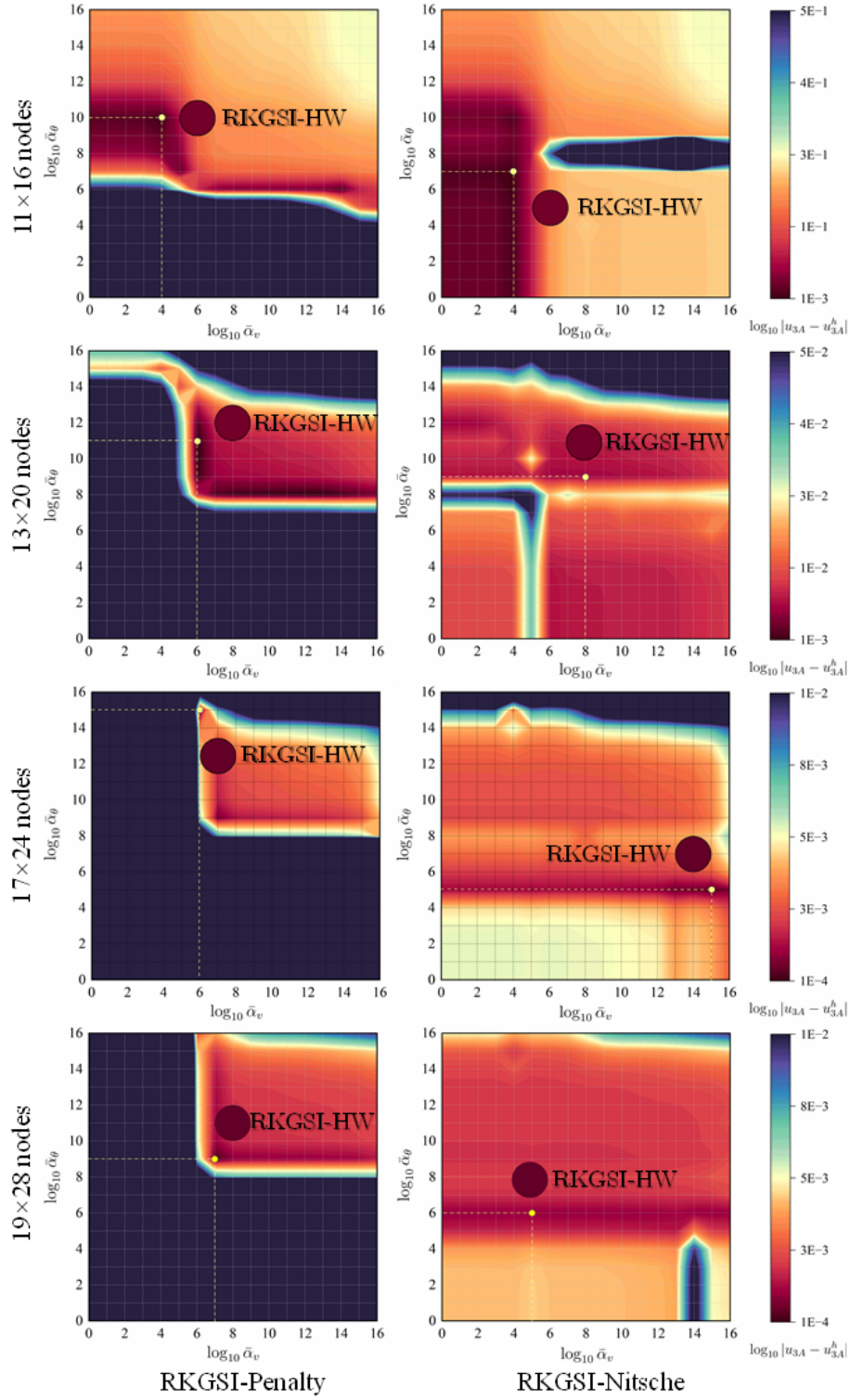


Figure 7: Sensitivity comparison of α_v and α_θ for Scordelis-Lo problem.

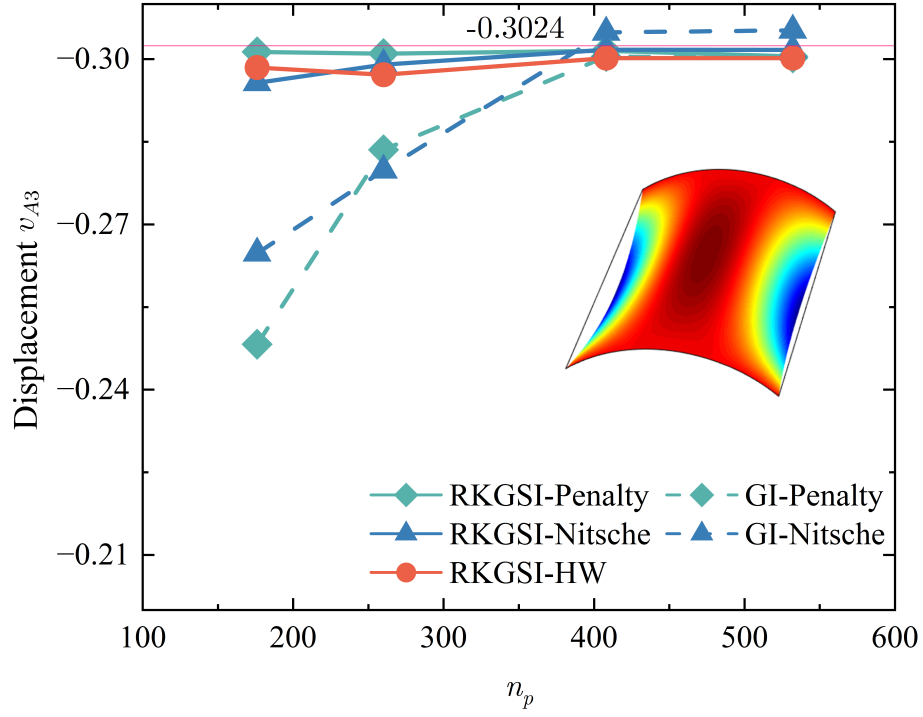


Figure 8: Displacement convergence for Scordelis-Lo roof problem.

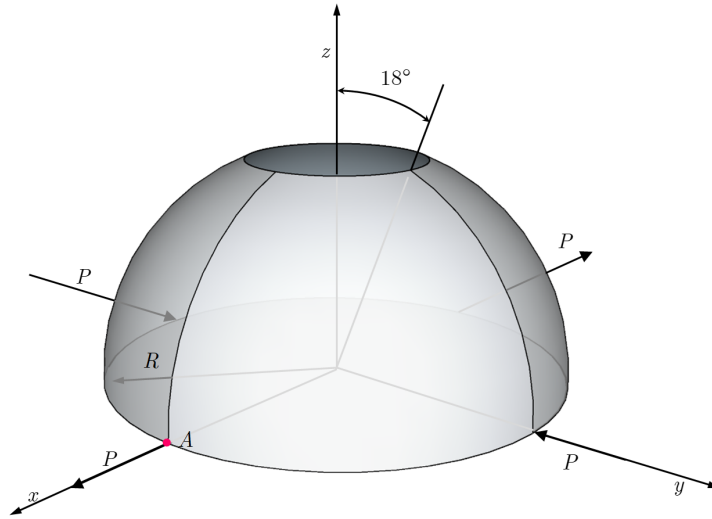
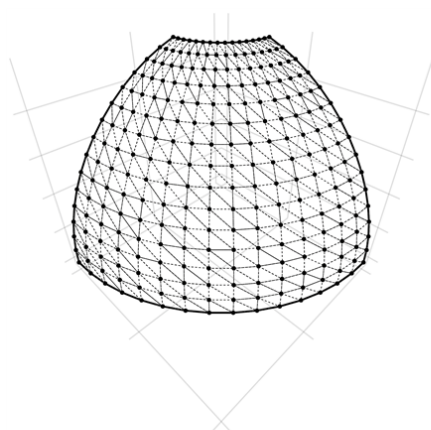
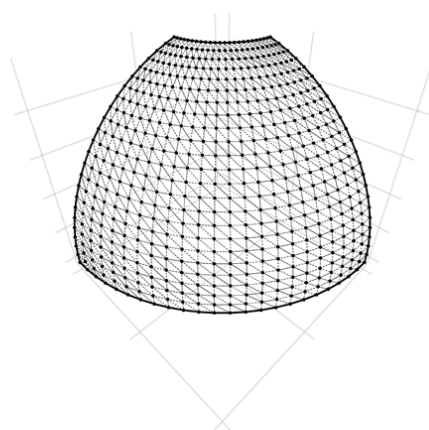


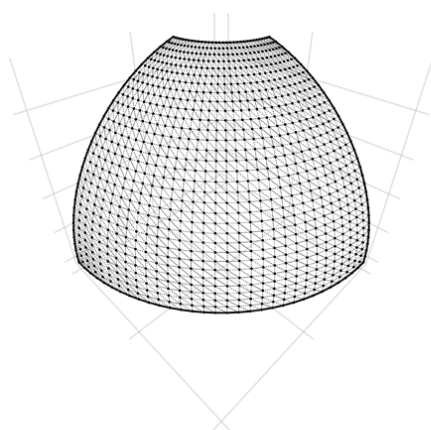
Figure 9: Description of pinched hemispherical shell problem.



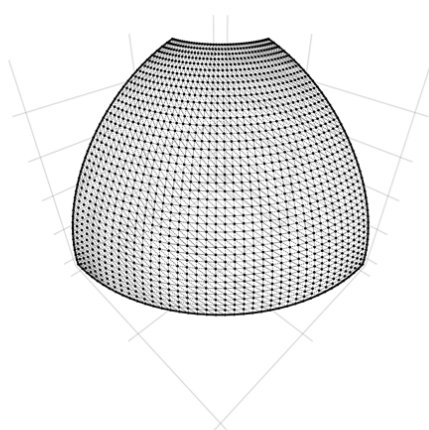
16×16 nodes



24×24 nodes



32×32 nodes



40×40 nodes

Figure 10: Meshfree discretizations for pinched hemispherical shell problem.

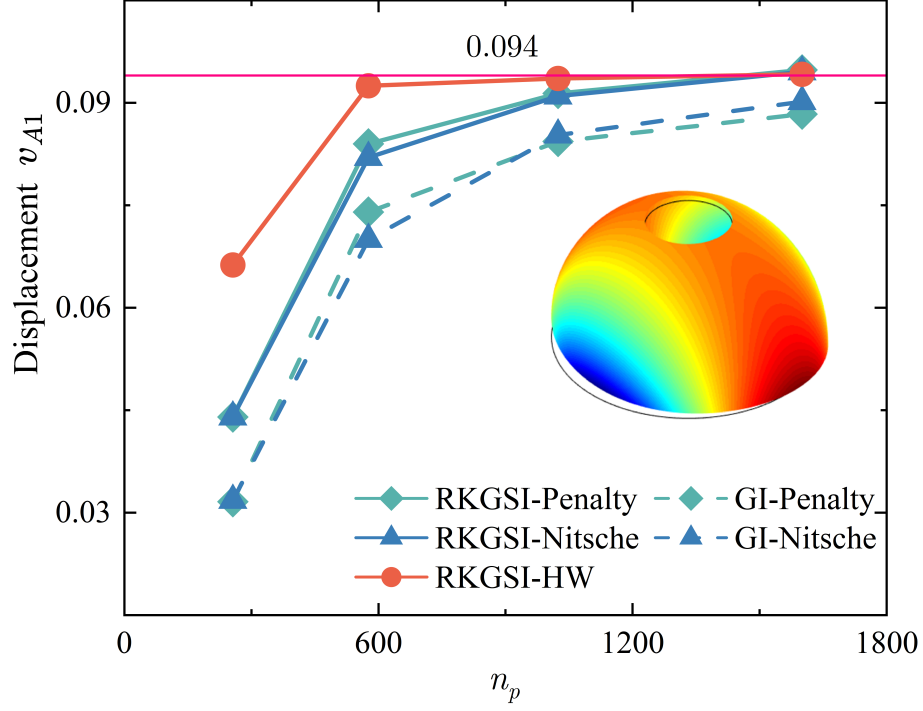


Figure 11: Displacement convergence for pinched hemispherical shell problem.

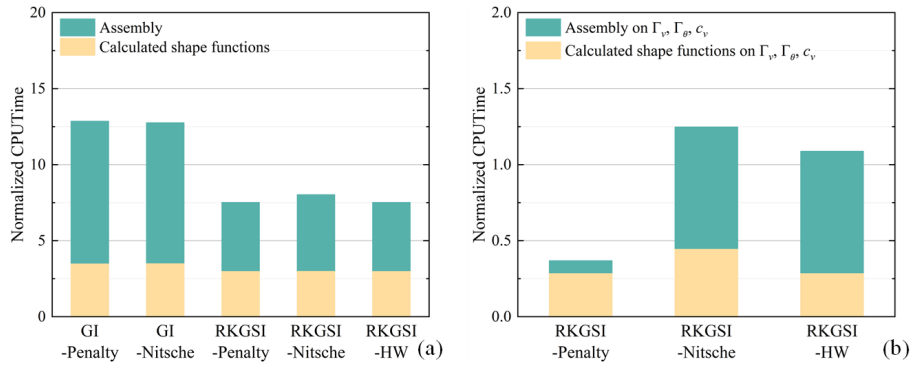


Figure 12: Efficiency comparison for pinched hemispherical shell problem: (a) Whole domain; (b) Essential boundaries

421 6. Conclusion

422 In this study, an efficient and quasi-consistent meshfree thin shell formu-
423 lation was presented to naturally enforce the essential boundary conditions.
424 Mixed formulation with the Hu-Washizu principle weak form is adopted, where
425 the traditional meshfree shape functions discretized the displacement, and the
426 strains and stresses were expressed by the reproducing kernel smoothed gradi-
427 ents and the covariant bases, respectively. The smoothed gradient naturally
428 embedded the first second-order integration constraints and has a quasi varia-
429 tional consistency for the curved models in each integration cell. Owing to the
430 Hu-Washizu variational principle, the essential boundary condition enforcement
431 has a similar form with the conventional Nitsche’s method; both have consistent
432 and stabilized terms. The costly high order derivatives in the Nitsche’s consis-
433 tent term have been replaced by the smoothed gradients, which improved the
434 computational speed due to the reproducing kernel gradient smoothing frame-
435 work. Furthermore, the stabilized term naturally existed in the Hu-Washizu
436 weak form, and the artificial parameter needed in Nitsche’s stabilized term has
437 vanished, which can automatically maintain the coercivity for the stiffness ma-
438 trix. Based on general reproducing kernel gradient smoothing framework, the
439 proposed methodology can be trivially extended to high order basis meshfree for-
440 mulation. The numerical results demonstrated that the proposed Hu-Washizu
441 quasi-consistent meshfree thin shell formulation showed excellent accuracy, ef-
442 ficiency, and stability.

Acknowledgment

The support of this work by the National Natural Science Foundation of China (12102138, 52350410467) and the Natural Science Foundation of Fujian Province of China (2023J01108, 2022J05056) is gratefully acknowledged.

447 Appendix A. Green's theorems for in-plane vector

448 This Appendix discusses two kinds of Green's theorems used for the devel-
 449 opment of the proposed meshfree method. For an arbitrary vectors v^α and a
 450 scalar function f , with Green's theorem for in-plane vector, the first Green's
 451 theorem is listed as follows [30]:

$$\begin{aligned} \int_{\Omega} f_{,\alpha} v^\alpha d\Omega &= \int_{\Gamma} f v^\alpha n_\alpha d\Gamma - \int_{\Omega} f (v_{,\alpha}^\alpha + \Gamma_{\beta\alpha}^\beta v^\alpha) d\Omega \\ &= \int_{\Gamma} f v^\alpha n_\alpha d\Gamma - \int_{\Omega} f v^\alpha|_\alpha d\Omega \end{aligned} \quad (\text{A.1})$$

452 where $\Gamma_{\alpha\beta}^\gamma = \mathbf{a}_{\alpha,\beta} \cdot \mathbf{a}^\gamma$ denotes the Christoffel symbol of the second kind. $v^\alpha|_\alpha$
 453 can be represented as the in-plane covariant derivative of the vector v^α :

$$v^\alpha|_\alpha = v_{,\alpha}^\alpha + \Gamma_{\beta\alpha}^\beta v^\alpha \quad (\text{A.2})$$

454 The second Green's theorem is established with a mixed form of second
 455 order derivative. Let $A^{\alpha\beta}$ can be an arbitrary symmetric second order tensor,
 456 the Green's theorem yields [30]:

$$\begin{aligned} \int_{\Omega} f_{,\alpha} A^{\alpha\beta} d\Omega &= \int_{\Gamma} f_{,\gamma} n^\gamma A^{\alpha\beta} n_\alpha n_\beta d\Gamma - \int_{\Gamma} f (A^{\alpha\beta} s_\alpha n_\beta)_{,\gamma} s^\gamma d\Gamma + [[f A^{\alpha\beta} s_\alpha n_\beta]]_{\mathbf{x} \in C} \\ &\quad - \int_{\Gamma} f (A_{,\beta}^{\alpha\beta} n_\alpha + \Gamma_{\alpha\beta}^\gamma A^{\alpha\beta} n_\gamma + \Gamma_{\gamma\beta}^\gamma A^{\alpha\beta} n_\alpha) d\Gamma \\ &\quad + \int_{\Omega} f \left(\Gamma_{\alpha\beta,\gamma}^\gamma A^{\alpha\beta} + \Gamma_{\alpha\beta}^\gamma A_{,\gamma}^{\alpha\beta} + \Gamma_{\eta\gamma}^\eta \Gamma_{\alpha\beta}^\gamma A^{\alpha\beta} \right. \\ &\quad \left. + A_{,\alpha\beta}^{\alpha\beta} + \Gamma_{\gamma\beta,\alpha}^\gamma A^{\alpha\beta} + 2\Gamma_{\gamma\alpha}^\gamma A_{,\beta}^{\alpha\beta} + \Gamma_{\gamma\alpha}^\gamma \Gamma_{\eta\beta}^\eta A^{\alpha\beta} \right) d\Omega \\ &= \int_{\Gamma} f_{,\gamma} n^\gamma A^{\alpha\beta} n_\alpha n_\beta d\Gamma - \int_{\Gamma} f (A^{\alpha\beta} s_\alpha n_\beta)_{,\gamma} s^\gamma d\Gamma + [[f A^{\alpha\beta} s_\alpha n_\beta]]_{\mathbf{x} \in C} \\ &\quad - \int_{\Gamma} f A^{\alpha\beta}|_\beta n_\alpha d\Gamma + \int_{\Omega} f A^{\alpha\beta}|_{\alpha\beta} d\Omega \end{aligned} \quad (\text{A.3})$$

457 with

$$A^{\alpha\beta}|_\beta = A_{,\beta}^{\alpha\beta} + \Gamma_{\beta\gamma}^\alpha A^{\beta\gamma} + \Gamma_{\gamma\beta}^\gamma A^{\alpha\beta} \quad (\text{A.4})$$

458

$$\begin{aligned} A^{\alpha\beta}|_{\alpha\beta} &= \Gamma_{\alpha\beta,\gamma}^\gamma A^{\alpha\beta} + \Gamma_{\alpha\beta}^\gamma A_{,\gamma}^{\alpha\beta} + \Gamma_{\eta\gamma}^\eta \Gamma_{\alpha\beta}^\gamma A^{\alpha\beta} \\ &\quad + A_{,\alpha\beta}^{\alpha\beta} + \Gamma_{\gamma\beta,\alpha}^\gamma A^{\alpha\beta} + 2\Gamma_{\gamma\alpha}^\gamma A_{,\beta}^{\alpha\beta} + \Gamma_{\gamma\alpha}^\gamma \Gamma_{\eta\beta}^\eta A^{\alpha\beta} \end{aligned} \quad (\text{A.5})$$

459 For the sake of brevity, the notion of covariant derivative is extended to a
 460 scalar function as:

$$f|_\alpha = f_{,\alpha} + \Gamma_{\beta\alpha}^\beta f \quad (\text{A.6})$$

461

$$f|_\beta n_\alpha = f_{,\beta} n_\alpha + \Gamma_{\alpha\beta}^\gamma f n_\gamma + \Gamma_{\gamma\beta}^\gamma f n_\alpha \quad (\text{A.7})$$

462

$$\begin{aligned} f|_{\alpha\beta} &= \Gamma_{\alpha\beta,\gamma}^\gamma f + \Gamma_{\alpha\beta}^\gamma f_{,\gamma} + \Gamma_{\eta\gamma}^\eta \Gamma_{\alpha\beta}^\gamma f \\ &\quad + f_{,\alpha\beta} + \Gamma_{\gamma\beta,\alpha}^\gamma f + 2\Gamma_{\gamma\alpha}^\gamma f_{,\beta} + \Gamma_{\gamma\alpha}^\gamma \Gamma_{\eta\beta}^\eta f \end{aligned} \quad (\text{A.8})$$

463 Appendix B. Derivations for stiffness metrics and force vectors

464 This Appendix details the derivations of stiffness matrices and force vectors
 465 in Eqs. (53)-(55), where the relationships of Eqs. (40), (41), (44) and (46) are
 466 used herein. Firstly, the membrane strain terms are considered as follows:

$$\begin{aligned}
 & \sum_{C=1}^{n_e} \int_{\Omega_C} \delta \tilde{\varepsilon}_{\alpha\beta}^h h C^{\alpha\beta\gamma\eta} \tilde{\varepsilon}_{\gamma\eta}^h d\Omega \\
 &= \sum_{C=1}^{n_e} \sum_{I,J=1}^{n_p} \delta \mathbf{d}_I \cdot \underbrace{\int_{\Omega_C} \tilde{\varepsilon}_{\alpha\beta I} h C^{\alpha\beta\gamma\eta} \mathbf{a}_\gamma \mathbf{q}^T d\Omega \mathbf{G}^{-1} \bar{\mathbf{g}}_{\eta J}}_{\tilde{\mathbf{g}}_I^{\eta T}} \cdot \mathbf{d}_J \\
 &= \sum_{C=1}^{n_e} \sum_{I,J=1}^{n_p} \delta \mathbf{d}_I \cdot \int_{\Gamma_C \cap \Gamma_v} \Psi_J \mathbf{q}^T \underbrace{\mathbf{G}^{-1} \tilde{\mathbf{g}}_I^\alpha n_\alpha}_{\tilde{\mathbf{T}}_{NI}} d\Gamma \cdot \mathbf{d}_J \\
 &= \sum_{I,J=1}^{n_p} \delta \mathbf{d}_I \cdot \int_{\Gamma_v} \tilde{\mathbf{T}}_{NI} \Psi_J d\Gamma \cdot \mathbf{d}_J
 \end{aligned} \tag{B.1}$$

467 with

$$468 \quad \tilde{\mathbf{g}}_I^\alpha = \mathbf{q} \mathbf{a}_\beta h C^{\alpha\beta\gamma\eta} \tilde{\varepsilon}_{\gamma\eta I} \tag{B.2}$$

$$469 \quad \tilde{\mathbf{T}}_{NI} = \mathbf{q}^T \mathbf{G}^{-1} \tilde{\mathbf{g}}_I^\alpha n_\alpha \tag{B.3}$$

Following this path, the bending strain terms can be reorganized by:

$$\begin{aligned}
 & \sum_{C=1}^{n_e} \int_{\Omega_C} \delta \tilde{\kappa}_{\alpha\beta}^h \frac{h^3}{12} C^{\alpha\beta\gamma\eta} \tilde{\kappa}_{\gamma\eta}^h d\Omega \\
 &= \sum_{C=1}^{n_e} \sum_{I,J=1}^{n_p} \delta \mathbf{d}_I \cdot \underbrace{\int_{\Omega_C} \tilde{\kappa}_{\alpha\beta I} \frac{h^3}{12} C^{\alpha\beta\gamma\eta} \mathbf{a}_3 \mathbf{q}^T d\Omega \mathbf{G}^{-1} \bar{\mathbf{g}}_{\gamma\eta J}}_{\tilde{\mathbf{g}}_I^{\gamma\eta T}} \cdot \mathbf{d}_J \\
 &= \sum_{C=1}^{n_e} \sum_{I,J=1}^{n_p} \delta \mathbf{d}_I \cdot \left(\begin{aligned} & \int_{\Gamma_C \cap \Gamma_\theta} \underbrace{\mathbf{q}^T \mathbf{G}^{-1} \tilde{\mathbf{g}}_I^{\alpha\beta} n_\alpha n_\beta}_{\tilde{\mathbf{M}}_{nnI}} n^\gamma \Psi_{J,\gamma} d\Gamma \\ & - \int_{\Gamma_C \cap \Gamma_v} \underbrace{(\mathbf{q}_{|\beta}^T \mathbf{G}^{-1} \tilde{\mathbf{g}}_I^{\alpha\beta} n_\alpha + (\mathbf{q}^T \mathbf{G}^{-1} \tilde{\mathbf{g}}_I^{\alpha\beta} s_\alpha n_\beta)_{,\gamma} s^\gamma)}_{\tilde{\mathbf{T}}_{MI}} \Psi_J d\Gamma \\ & + [[\underbrace{\mathbf{q}^T \mathbf{G}^{-1} \tilde{\mathbf{g}}_I^{\alpha\beta} s_\alpha n_\beta}_{\tilde{\mathbf{P}}_I \mathbf{a}_3} \Psi_J]]_{\mathbf{x} \in C_C \cap C_v} \end{aligned} \right) \cdot \mathbf{d}_J \\
 &= \sum_{I,J=1}^{n_p} \delta \mathbf{d}_I \cdot \left(\int_{\Gamma_\theta} \tilde{\mathbf{M}}_{nnI} n^\gamma \Psi_{J,\gamma} d\Gamma - \int_{\Gamma_v} \tilde{\mathbf{T}}_{MI} \Psi_J d\Gamma + [[\tilde{\mathbf{P}}_I \Psi_J]]_{\mathbf{x} \in C_v} \right)
 \end{aligned} \tag{B.4}$$

470 with

$$\tilde{\mathbf{g}}_I^{\alpha\beta} = \int_{\Omega_C} \mathbf{q} \frac{h^3}{12} C^{\alpha\beta\gamma\eta} \mathbf{a}_3 \tilde{\kappa}_{\gamma\eta I} d\Omega \quad (\text{B.5})$$

471

$$\begin{cases} \tilde{M}_{nnI} = \mathbf{q}^T \mathbf{G}^{-1} \tilde{\mathbf{g}}_I^{\alpha\beta} n_\alpha n_\beta \\ \tilde{\mathbf{T}}_{MI} = \mathbf{q}_{|\beta}^T \mathbf{G}^{-1} \tilde{\mathbf{g}}_I^{\alpha\beta} n_\alpha + (\mathbf{q}^T \mathbf{G}^{-1} \tilde{\mathbf{g}}_I^{\alpha\beta} s_\alpha n_\beta)_{,\gamma} s^\gamma \\ \tilde{\mathbf{P}}_I = \mathbf{q}^T \mathbf{G}^{-1} \tilde{\mathbf{g}}_I^{\alpha\beta} s_\alpha n_\beta \cdot \mathbf{a}_3 \end{cases} \quad (\text{B.6})$$

472 References

- 473 [1] L. H. Donnell, Beams, Plates and Shells, McGraw-Hill, 1976.
- 474 [2] T. J. Hughes, The Finite Element Method: Linear Static and Dynamic
475 Finite Element Analysis, Dover Publications, Mineola, New York, 2000.
- 476 [3] T. Belytschko, Y. Y. Lu, L. Gu, Element-free Galerkin methods, Interna-
477 tional Journal for Numerical Methods in Engineering 37 (1994) 229–256.
- 478 [4] W. K. Liu, S. Jun, Y. F. Zhang, Reproducing kernel particle methods,
479 International Journal for Numerical Methods in Fluids 20 (1995) 1081–
480 1106.
- 481 [5] J. S. Chen, M. Hillman, S. W. Chi, Meshfree methods: Progress made after
482 20 Years, Journal of Engineering Mechanics 143 (2017) 04017001.
- 483 [6] P. Krysl, T. Belytschko, Analysis of thin shells by the Element-Free
484 Galerkin method, International Journal of Solids and Structures 33 (1996)
485 3057–3080.
- 486 [7] G. R. Liu, Meshfree Methods: Moving Beyond the Finite Element Method,
487 Second Edition, Crc Press, 2009.
- 488 [8] X. Zhang, K. Z. Song, M. W. Lu, X. Liu, Meshless methods based on
489 collocation with radial basis functions, Computational Mechanics 26 (2000)
490 333–343.
- 491 [9] D. Millán, A. Rosolen, M. Arroyo, Thin shell analysis from scattered points
492 with maximum-entropy approximants, International Journal for Numerical
493 Methods in Engineering 85 (2011) 723–751.
- 494 [10] L. Wang, M. Hu, Z. Zhong, F. Yang, Stabilized Lagrange Interpolation
495 Collocation Method: A meshfree method incorporating the advantages of
496 finite element method, Computer Methods in Applied Mechanics and En-
497 gineering 404 (2023) 115780.
- 498 [11] P. Suchde, T. Jacquemin, O. Davydov, Point Cloud Generation for Mesh-
499 free Methods: An Overview, Archives of Computational Methods in Engi-
500 neering 30 (2022) 889–915.
- 501 [12] L. Deng, D. Wang, An accuracy analysis framework for meshfree collocation
502 methods with particular emphasis on boundary effects, Computer Methods
503 in Applied Mechanics and Engineering 404 (2023) 115782.
- 504 [13] J. Wang, M. Hillman, Upwind reproducing kernel collocation method for
505 convection-dominated problems, Computer Methods in Applied Mechanics
506 and Engineering 420 (2024) 116711.

- 507 [14] S. Fernández-Méndez, A. Huerta, Imposing essential boundary conditions
508 in mesh-free methods, *Computer Methods in Applied Mechanics and En-*
509 *gineering* 193 (2004) 1257–1275.
- 510 [15] X. Li, Error estimates for the moving least-square approximation and the
511 element-free Galerkin method in n-dimensional spaces, *Applied Numerical*
512 *Mathematics* 99 (2016) 77–97.
- 513 [16] J. Wu, D. Wang, An accuracy analysis of Galerkin meshfree methods ac-
514 counting for numerical integration, *Computer Methods in Applied Mechan-*
515 *ics and Engineering* 375 (2021) 113631.
- 516 [17] J. S. Chen, H. P. Wang, New boundary condition treatments in meshfree
517 computation of contact problems, *Computer Methods in Applied Mechan-*
518 *ics and Engineering* 187 (2000) 441–468.
- 519 [18] D. Liu, Y. M. Cheng, The interpolating element-free Galerkin (IEFG)
520 method for three-dimensional potential problems, *Engineering Analysis*
521 *with Boundary Elements* 108 (2019) 115–123.
- 522 [19] V. Ivannikov, C. Tiago, P. M. Pimenta, On the boundary conditions of the
523 geometrically nonlinear Kirchhoff–Love shell theory, *International Journal*
524 *of Solids and Structures* 51 (2014) 3101–3112.
- 525 [20] Y. Y. Lu, T. Belytschko, L. Gu, A new implementation of the element free
526 Galerkin method, *Computer Methods in Applied Mechanics and Engineer-*
527 *ing* 113 (1994) 397–414.
- 528 [21] T. Zhu, S. N. Atluri, A modified collocation method and a penalty formu-
529 lation for enforcing the essential boundary conditions in the element free
530 Galerkin method, *Computational Mechanics* 21 (1998) 211–222.
- 531 [22] S. Skatulla, C. Sansour, Essential boundary conditions in meshfree methods
532 via a modified variational principle: Applications to shell computations,
533 *Computer Assisted Mechanics and Engineering Sciences* 15 (2008) 123–142.
- 534 [23] J. S. Chen, C. T. Wu, S. Yoon, Y. You, A stabilized conforming nodal
535 integration for Galerkin mesh-free methods, *International Journal for Nu-*
536 *merical Methods in Engineering* 50 (2001) 435–466.
- 537 [24] J. S. Chen, M. Hillman, M. Rüter, An arbitrary order variationally consis-
538 tent integration for Galerkin meshfree methods, *International Journal for*
539 *Numerical Methods in Engineering* 95 (2013) 387–418.
- 540 [25] Q. Duan, X. Li, H. Zhang, T. Belytschko, Second-order accurate derivatives
541 and integration schemes for meshfree methods, *International Journal for*
542 *Numerical Methods in Engineering* 92 (2012) 399–424.

- 543 [26] D. Wang, J. Wu, An inherently consistent reproducing kernel gradient
544 smoothing framework toward efficient Galerkin meshfree formulation with
545 explicit quadrature, *Computer Methods in Applied Mechanics and Engi-*
546 *neering* 349 (2019) 628–672.
- 547 [27] J. Wang, X. Ren, A consistent projection integration for Galerkin meshfree
548 methods, *Computer Methods in Applied Mechanics and Engineering* 414
549 (2023) 116143.
- 550 [28] J. Wu, X. Wu, Y. Zhao, D. Wang, A consistent and efficient method for
551 imposing meshfree essential boundary conditions via hellinger-reissner vari-
552 ational principle., *Chinese Journal of Theoretical and Applied Mechanics*
553 54 (2022) 3283–3296.
- 554 [29] J. Wu, X. Wu, Y. Zhao, D. Wang, A rotation-free Hellinger-Reissner mesh-
555 free thin plate formulation naturally accommodating essential boundary
556 conditions, *Engineering Analysis with Boundary Elements* 154 (2023) 122–
557 140.
- 558 [30] J. Benzaken, J. A. Evans, S. F. McCormick, R. Tamstorf, Nitsche’s method
559 for linear Kirchhoff–Love shells: Formulation, error analysis, and verifica-
560 tion, *Computer Methods in Applied Mechanics and Engineering* 374 (2021)
561 113544.
- 562 [31] H. Dah-wei, A method for establishing generalized variational principle,
563 *Applied Mathematics and Mechanics* 6 (1985) 501–509.
- 564 [32] H. Du, J. Wu, D. Wang, J. Chen, A unified reproducing kernel gradient
565 smoothing Galerkin meshfree approach to strain gradient elasticity, *Com-*
566 *putational Mechanics* 70 (2022) 73–100.
- 567 [33] J. Kiendl, K. U. Bletzinger, J. Linhard, R. Wüchner, Isogeometric shell
568 analysis with Kirchhoff–Love elements, *Computer Methods in Applied Me-*
569 *chanics and Engineering* 198 (2009) 3902–3914.
- 570 [34] R. H. Macneal, R. L. Harder, A proposed standard set of problems to test
571 finite element accuracy, *Finite Elements in Analysis and Design* 1 (1985)
572 3–20.